**Supplementary Material Index:**

- Supplemental Materials and Methods.
- Supplemental Figures:
  - Supplemental Figure 1: *Overall workflow of ex vivo chemosensitivity assay.*
  - Supplemental Figure 2: *Computational implementation of tumor sensitivity as a probability distribution*.
  - Supplemental Figure 3: *Spatial co-localization of MM and stroma*.
  - Supplemental Figure 4: *Example of assessment of spontaneous cell death in 14 primary MM samples across 96h in EMMA's ex vivo assay*.
  - Supplemental Figure 5: *Ex vivo chemosensitivity curve of patient Pt103 to carfilzomib*.
  - Supplemental Table 1: *Model parameters for patient Pt103's primary MM cells tested ex vivo with carfilzomib*.
  - Supplemental Figure 6: *Correlation between predicted trajectories and actual clinical response of 52 MM patients up to 90 days post biopsy*.
  - Supplemental Table 2: *Choice of best therapeutic option based on EMMA*.
  - Supplemental Figure 7: *Correlation between ex vivo drug efficacy in 12 MM patients tested with six chemotherapeutic agents and 25 PKIs*.
  - Supplemental Figure 8: *Hypothetical models for inter-patient correlation of drug sensitivity*.
  - Supplemental Figure 9: *Changes in chemosensitivity of tumor cells from two MM patients to 20 PKIs between two sequential biopsies*.
  - Supplemental Figure 10: *Model predictions of 41 MM patients indicate no correlation between bortezomib and carfilzomib 90-day depth of response*.
  - *Supplemental Table 3: Demographics of patients whose bone marrow aspirates were used in virtual clinical trials of ricolinostat and venetoclax.*
  - Supplemental Figure 11: *Quantification of drug sensitivity and time-dependent synergy in primary MM cells.*
  - Supplemental Figure 12: *Daratumumab-mediated MM cell death.*
  - Supplemental Figure 13: *Ex vivo chemosensitivity in sequential biopsies in absence and during treatment*.
  - Supplemental Figure 14: *Intra-plate variation of ex vivo assay*.
  - Supplemental Figure 15: *Convergence study comparing the four population models for panobinostat*.
  - Supplemental Table 4: *SSR, number of parameters, and AIC values for the four models for patient Pt103's ex vivo sensitivity to panobinostat*.
  - Supplemental Figure 16: *Convergence study comparing the four population models for carfilzomib*.
  - Supplemental Table 5: *SSR, number of parameters, and AIC values for the four models for patient Pt103's ex vivo sensitivity to carfilzomib*.
  - Supplemental Figure 17: *Comparison between clinical predictions for bortezomib using the four models*.
  - Supplemental Figure 18: *Comparison between clinical predictions for carfilzomib using the four models*.
- Data Processing Guide:
- Java and Matlab source code are available at the PI's website: http://www.i-genics.com/SilvaShain2015. De-identified patient drug sensitivity files are available at Synapse.org under doi:10.7303/syn7843820

## Supplemental Materials and Methods:

***A novel platform for analysis of drug combinations.*** One of the goals of this study was to develop a platform capable of testing a large number of potential therapeutic agents and combinations (clinical utility and drug development), while maintaining the level of detail required by the mathematical model to simulate the clinical efficacy of each agent or combination. For this purpose, regular drug interaction analysis at a fixed time point is not sufficient, as the temporal effect must be captured into the mathematical model. **Supplemental Figures 11a** and **11b** depict the LD50s (concentration required to kill 50% of MM cells) for primary MM cells from two patients to a panel of drugs and combinations. Despite being a useful representation of patient-specific drug efficacy as single agents, these classic bar plots provide only limited interpretation of the dynamics of drug interaction, and they do not incorporate critical time-dependent information. **Supplemental Figures 11c** and **11d** exemplify how this assay can be used to determine the cell-kill benefit of combining two agents. Each image represents normalized drug concentration on the horizontal axis and exposure time on the vertical axis (h). The color range represents the increase in percentage of cell death of the agent combination as compared to cell death induced by a single agent (values above 20% are red; negative values are blue). **Supplemental Figure 11c** shows that, for the first patient, bortezomib combined with panobinostat (HDACi), had a significant increase in cell-kill as compared to bortezomib alone at all concentrations, with highest benefit in the lowest concentrations. The benefit of bortezomib plus panobinostat relative to single agent panobinostat is restricted mainly to the lowest concentrations. The lowest panel of **Supplemental Figure 11c** depicts the regions of synergy or the area in which the cell-kill of the combination of bortezomib and panobinostat is higher than the Bliss additive[1] effect of both drugs. Similar data for the second patient are presented in **Supplemental Figure 11d** and illustrate the response pattern of CRM1i plus doxorubicin. Synergy between bortezomib and panobinostat[2] as well as CRM1i and doxorubicin[3] have been previously identified, but the graphs from **Supplemental Figures 11c** and **11d** show evidence of how these positive interactions can be limited to a small range of concentrations and narrow windows of time. As such, it appears that synergy is difficult to identify and interpret by classical methods[4,5]. This is especially true for primary cells, where the number of experimental conditions that can be tested in a single sample is limited.

To study drug interactions in patient samples, we have added two drugs at maximum concentration and diluted them serially, so that their concentration ratio remains the same across all wells tested. To assess the benefit of adding panobinostat to a bortezomib regimen for a particular patient, we have subtracted the dose response surface of bortezomib from the dose response surface of the combination. The result is depicted in **Supplemental Figure 11c**, top panel, showing in red the conditions (concentration and exposure time) where the difference in cell kill is higher than 20%. Regions where the increase in cell kill is negligible or negative are shown in blue, and a color gradient is used for the intermediate values. Here we use the classic definition of synergy, which determines that two drugs are synergistic if their combined effect (percent cells killed) is higher than the combination of their independent effect[1]. For instance, consider that drugs A and B, at a specific concentration and during a certain period of time, kill the fractions $a$ and $b$ of cells, where $a<1$ and $b<1$. Should the combination of both drugs kill a fraction equal to $[1-(1-a)*(1-b)]$, then A and B are additive. If the fraction killed is higher, the drugs are synergistic; if lower, they are antagonistic.

***Determination of variation of ex vivo chemosensitivity between sequential samples (test-retest).*** One of the most important components of this assay is the capture of changes in a patient's clinical response over time (sequential therapy). First, we have performed a test-retest in order to assess the inter-day variability of the assay. This variability includes, but is not limited to: inter-day variation of media and reagents, biopsy procedure, MM cell enrichment, plate seeding and drugging with robotic plate handler, sequential imaging, and digital image analysis. **Supplemental Figure 13a** depicts the clinical history of a MM patient who had two biopsies performed within one month, in absence of treatment. We have quantified the chemosensitivity of both biopsies and used this information to build mathematical models of clinical response (red dashed line for

data from biopsy 1, blue solid line for data from biopsy 2) to the therapy the patient ultimately received after the second biopsy (CRM1i + liposomal doxorubicin). Results indicated high correlation between both modeled curves (Pearson r=0.9707) demonstrating reproducibility of the assay, as well as accuracy of predicted depth of response and actual outcome (solid green line). **Supplemental Figure 13b** represents a measure of the inter-day variability of this assay, which is the predicted best clinical response through 90 days, demonstrating inter-day consistency of model predictions.

We also evaluated the influence of therapy on *ex vivo* drug sensitivity in sequential biopsy analyses. **Supplemental Figure 13c** represents a patient with two sequential biopsies separated by five months (**Pt32**). During the intervening period, the patient was treated with a combination of a hypoxia-activated alkylating agent (TH-302), proteasome inhibitor (bortezomib) and immunomodulatory agent (dexamethasone), leading to a partial response followed by relapse. The clinical predictions generated by the mathematical model based on the first biopsy (pre-treatment) indicated that this patient was highly sensitive to bortezomib and melphalan, moderately sensitive to CRM1i, and refractory to liposomal doxorubicin (**Supplemental Figure 13d**). The mathematical models parameterized by the biopsy post-relapse indeed confirm that the tumor has become refractory to bortezomib, maintained its resistance to liposomal doxorubicin, and would present only a minor response to melphalan or CRM1 inhibitor. These data demonstrate the ability of the *ex vivo* model to account for the changing drug resistant subpopulations associated with intervening therapy suggesting that this platform has the potential to provide meaningful information as a clinical decision support tool throughout the course of a patient's cycles of clinical management.

***Determination of intra-plate variation.*** We have characterized the behavior of this assay towards intra-plate variability. It is well known that temperature and gas gradients contribute to location bias in multi-well plates. In order to determine the degree of intra-plate variation or possible spatial bias, we plated primary MM cells from one patient (Pt48, **Supplemental Figure 14**) in co-culture with patient-derived stroma embedded in collagen matrix and repeated a pattern of 3 drugs (melphalan, bortezomib and carfilzomib) as well as negative control, eight times across the plate. Each drug was tested in five different concentrations and two replicates. There were also positive controls for each drug (cell lines at highest concentration, two replicates). We have grouped the measurements of both replicates of each concentration for each drug in each of the eight repeats across the plate. Similarly, we have also grouped and determined the variation in the negative and positive controls. In order to determine the contribution of location in the plate versus exposure time, we have calculated a two-way ANOVA on each combination of drug-concentration (total of 16 ANOVAs). For the control and low concentrations, where there is no measurable drug-induced cell death, the contribution of both exposure time and location in plate should be similar, and the total variation should be negligible. However, for higher drug concentrations, we expected most of the variation to come from exposure time and only a negligible amount to be attributed to location in the plate. In the control wells, 41% of the variation came from exposure time and 36% from location. For the highest concentrations of bortezomib, carfilzomib and melphalan, these values were 99%, 98% and 97% for exposure time, <1%, 2% and 2% for location. Also, as expected, the total variation, quantified as the total sum of squares (SS) in the highest concentrations for bortezomib, carfilzomib and melphalan, were 58-, 50- and 39-fold higher than control, respectively. These test-retest studies demonstrate that the assay is robust with low intra-plate variation.

***Convergence of solution for parameters of ex vivo chemosensitivity.*** **Supplemental Figure 15** shows MATLAB's l*sqcurvefit* converge to the parameter estimates as it approaches a minimal value of *SSR* for the four models fitted to the *ex vivo* data for panobinostat. The single population, no distribution model, as referenced in **Supplemental Table 4**, is the model with the smallest AIC value. Even though the "two-population with distribution" is the model with the least SSR, indicating that the benefit in terms of SSR is marginal as compared to adding additional parameters to the model. It can also be observed that all parameters in the single population model quickly converge and stabilize, while both 2-population models show oscillation of parameters, indicating an underdetermined system.

**Supplemental Figure 16** shows MATLAB's l*sqcurvefit* converge to the parameter estimates as it approaches a minimal value of *SSR* for the four population models fitted to the *ex vivo* data for carfilzomib. The best model chosen based on the least AIC is the one with two populations modeled as distributions as shown in **Supplemental Table 5**. Note the considerable reduction in SSR between two population and one population models, as well as the stability of the parameter values after convergence, validating heterogeneity in tumor population.

**Supplemental Figure 17** depicts a comparison between the clinical predictions for Pt103 using the four different models for bortezomib. Notice the similarity in the clinical predictions and the AIC values. This is a case where all the proposed models fit the data sufficiently well and we choose the model with the least AIC. On the other hand, **Supplemental Figure 18** presents a comparison between the clinical predictions for Pt103 using the four models for carfilzomib. Notice the variation in clinical predictions between the models. This is a case where AIC chooses the model that fits the data best (lowest SSR), two populations modeled as distributions. In summary, the choice of the correct, simplest model, may lead to significant differences in the clinical outcome.

***Extended Description of Mathematical Model.*** We propose a nonlinear dynamical model to describe the growth/death of tumor populations in MM patients. For this purpose, we employ a statistical, grey-box, parametric model that represents the tumor's response to various drugs by modeling them as a distribution of populations, where each subpopulation has a different level of sensitivity to a given drug concentration. Further, within a subpopulation it is assumed that the likelihood of cell death depends on the drug concentration.

Let the total number of MM cells in the patient's body be quantified and represented by *p(t)*, which stands for population of tumor cells. The tumor burden, in the absence of treatment, is assumed to increase with time due to cell replication.

The non-monotonic variation of the tumor population was modeled as a difference equation

$$p(t+dt) = p(t)G(dt)D(t,dt), \qquad \text{(Equation S1)}$$

where *G(dt)* is the growth factor due to tumor cell replication and *D(t,dt)* is the death factor due to drug-induced cell death between times *t* and *t+dt*.

*Tumor growth in absence of therapy.* In cell culture, the time required for the number of cells in a flask to double, commonly known as doubling time, is used as a metric for quantifying growth due to cell replication. For mammalian cells this number is often around 24 hours. However, the doubling time of MM tumors is much longer due to its characteristically low proliferative index. In the mathematical model, the growth factor for the MM population in the absence of therapy is:

$$G(dt) = \left(1 + LI\left(2^{\Delta t} - 1\right)\right)^{dt/\Delta t}, \qquad \text{(Equation S2)}$$

where *dt* is a time interval (in days) between measurements, labeling index *LI* is the percentage of MM cells actively replicating, and $\Delta t$ is the time step used during simulation.

Let a given patient have a *LI* of 3% and say we would like to determine the growth of the tumor over a period of three days. Using Equation 2 with a *LI* of 0.03, *dt* of 3 days, and $\Delta t$ of 5 minutes or 1/288 days:

$$G(3) = \left(1 + 0.03\left(2^{1/288} - 1\right)\right)^{3\times 288} = 1.064.$$

Thus, the MM population, or tumor burden, would increase 6.4% in three days for this patient. Conversely, to determine *LI* for a given patient, we use a method similar to the calculation of doubling time in cell culture. We use the two closest prior measures of tumor burden as obtained from monoclonal paraprotein, a surrogate of tumor burden in MM, and use Equations S1 and S2 to determine *LI*. For example, prior to the current biopsy, a MM patient had two measures of Serum-free light chain (lambda) confirming relapse, where the first was 996mg/L and the second measure was 1,312mg/L, 34.2 days later. Thus, *LI* can be calculated as:

$$LI = \frac{\left(\frac{p(t+dt)}{p(t)}\right)^{\Delta t/dt} - 1}{\left(2^{\Delta t} - 1\right)} = \frac{\left(1312/996\right)^{1/(288\times 34.2)} - 1}{\left(2^{1/288} - 1\right)} = 0.0116, \text{ or } 1.16\%.$$

*Therapy-induced death of tumor cells.* Prior to modeling the stochastic cell death process, we have proposed an empirical pharmacodynamics model based on the drug occupancy theory, described by the reaction [6]

$$\left[\text{Drug}\right] + \left[\text{Receptor}\right] \underset{\text{Dissociation}}{\overset{\text{Binding}}{\rightleftharpoons}} \left[\begin{array}{c}\text{Drug-Receptor}\\ \text{Complex}\end{array}\right] \xrightarrow{\text{Threshold}} \text{Response},$$

where drug and receptor molecules form drug-receptor complexes, which in turn cause cellular damage and, beyond a certain threshold, initiates cell death. The dynamics of this reversible reaction follows

$$\frac{d\beta}{dt} = \underbrace{-\kappa\,\beta(t)}_{\text{Dissociation}} + \underbrace{\delta\,R(t)^h}_{\text{Binding}},$$

(Equation S3)

where, the forward rate of reaction is given by the law of mass action [7] and is described as the rate of binding alone

$$\left.\frac{d\beta}{dt}\right|_f = \left(K_f\left[\text{Receptor}\right]^s\right)R(t)^h = \delta\,R(t)^h,$$

(Equation S4)

where, *R(t)* is the drug concentration at time *t*. *s* and *h* are stoichiometric coefficients of the reversible reaction. Further the rate of dissociation is proportional to the extent of binding $\beta(t)$ and and an empirical rate constant $\kappa$. Equation S3 is in Bernoulli's ODE form and has an analytical solution assuming binding starts at t=0.

$$\beta(t) = \delta\int_0^t e^{-\kappa(t-T)}R(T)^h dT,$$

(Equation S5)

When the cellular damage is greater than the threshold, the probability of cell death increases asymptotically with increase in damage as in a sigmoid function

$$y(x) = 1 - \frac{1}{1+e^{-\sigma x}},$$

(Equation S6)

Where *e* is the Euler's number and $\sigma$ is a positive number defining the steepness of the curve. As the probability of cell death cannot be negative, Equation S6 was modified such that the death function *D* varies from 1 to 0.5 as the accumulated binding beyond the threshold varies from 0 to $\infty$:

$$D(t,dt) = 1 - 0.5\tanh\left(\alpha(t)/2\right)dt,$$

(Equation S7)

$$\alpha(t,dt) = \max\left(\frac{\beta(t,dt)-\tau}{\delta}, 0\right)$$

(Equation S8)

where $\alpha$ is a measure of accumulated damage beyond the threshold, $\tau$, and $\delta$ is a non-dimensionalizing empirical factor.

*Modeling heterogeneity in tumor population.* The short-term response of MM patients to therapy can be monotonic (continuous increase or decrease of tumor burden), or may present an inflexion point followed by relapse (**Figure 2a-c**). Thus, the tumor chemosensitivity of MM patients cannot always be accurately described by a single "clonal" population, but requires a more general representation. In this model, we propose the tumor composed of two subpopulations, with different degrees of sensitivity to therapy. Each subpopulation

can either be modeled as "clonal" or as a distribution, with drug-specific threshold values ($\tau$, Equation S8). These threshold values are obtained from a normally distributed probability density function (defined in terms of a drug-specific mean and variance) that specifies the fraction of a subpopulation that initiates cell death beyond a given threshold. The rationale behind adopting such an approach lies in the assumption that both sensitive and resistant subpopulations have their own degree of heterogeneity. **Figure 2b** shows an example of such a representation of tumor chemosensitivity as a single and as a double distribution.
The total tumor burden of a patient is

$$p(t+dt) = \sum_{j=1}^{2} p_j(t+dt), \quad j = 1,2 \text{ subpopulations}, \qquad \text{(Equation S9)}$$

where the composition of each subpopulation at initial time $t_0$ is modeled as a distribution

$$PDF\left(\tau; \mu_j, {\sigma_j}^2\right) = \frac{1}{\sqrt{2\pi {\sigma_j}^2}} \exp\left(-\frac{\left(\tau - \mu_j\right)^2}{{\sigma_j}^2}\right) \qquad \text{(Equation S10)}$$

with a specific mean $\mu_j$ and standard deviation $\sigma_j$ that define the percentage of cells that initiate cell death when the accumulated damage surpasses $\tau$. For computational purposes, we have discretized this distribution in a histogram with *n* bins, ranging from $\mu_j - 6\sigma_j$ to $\mu_j + 6\sigma_j$, using MATLAB's function *normpdf* (**Supplemental Figure 2**).

$$p_{j,i}(t+dt) = p_{j,i}(t) G(dt) D_j(t, dt, \tau_i), \quad j = 1,2 \text{ subpoplations. } i = 1,\ldots,n \text{ bins.} \qquad \text{(Equation S11)}$$

$$p_j(t+dt) = \sum_{i=1}^{n} p_{j,i}(t+dt), \quad j = 1,2 \text{ subpopulations. } i = 1,\ldots,n \text{ bins.} \qquad \text{(Equation S12)}$$

There is no biological meaning for negative $\tau$ values, so the histogram is truncated when $\mu_j - 6\sigma_j < 0$, and the value of each bin is normalized so that the sum of all bins corresponds to $p_j$. Thus, at initial time $t_0$, the composition of the $j^{th}$ subpopulation

$$p_{j,i}(t_0) \approx \frac{\hat{p}_{j,i}(t_0)}{\sum_{i=1}^{n} \hat{p}_{j,i}(t_0)} \times p_j(t_0), \qquad j = 1,2 \text{ subpopulations. } i = 1,\ldots,n \text{ bins}, \qquad \text{(Equation S13)}$$

where $\hat{p}_{j,i}(t_0) = \begin{cases} PDF\left(\tau_i; \mu_j, \sigma_j\right), & \forall \tau_i \geq 0 \\ 0, & \forall \tau_i < 0 \end{cases}$

In summary, the model assumes the existence of two tumor subpopulations, with different degrees of chemosensitivity. Each subpopulation, in turn, exhibits a range of sensitivity to therapy modeled as a normally distributed probability density function. The total number of parameters for this general model is nine: two subpopulation-specific mean and standard deviation, two reaction constants $\delta$, one drug-specific cell repair rate $\kappa$, one drug-specific empirical parameter *h* relating drug concentration to response, and the ratio of sensitive population to the entire tumor population.

In specific cases, the estimated standard deviation may be so small that it may be beneficial to model one subpopulation as a Dirac delta function. In such a case, the threshold $\tau$ could be estimated directly, reducing the total number of parameters of the system to seven. Additionally, one of the populations may be so small that its effect cannot be detected by the *ex vivo* assay, and thus the tumor could be modeled as only one population.

*Determining model parameters for a specific drug-patient combination.* Before predicting the clinical response of MM patients using the proposed model, we need to, firstly, estimate the parameters for all the models specified above using *ex vivo* data, and secondly, choose the model that best fits the data. One of the challenges faced in dealing with *ex vivo* data is to ensure that it best represents tumor response *in vivo*. An

important point in this process is to differentiate between drug-induced cell death, *D(t,dt)* in Equation 1, and spontaneous *ex vivo* cell death. This is accomplished by normalizing the *ex vivo* response of the tumor to a specific concentration of a drug with the *ex vivo* vehicle control. Let

$$p_{R_x}(t+dt) = \left( p_{R_x}(t) D_e(t,dt) \right) G(dt) D(t,dt) \quad \text{(Equation S14)}$$

represent the response of tumor to drug $R_x$ *ex vivo*, where $D_e(t,dt)$ represents the rate of spontaneous cell death. Further, let

$$p_c(t+dt) = p_c(t) G(dt) D_e(t,dt) \quad \text{(Equation S15)}$$

represent the *ex vivo* behavior of the control. By dividing Equations S14 and S15, we have

$$\frac{p_{R_x}(t+dt)}{p_c(t+dt)} = \left( \frac{p_{R_x}(t)}{p_c(t)} \right) D(t,dt), \quad \text{(Equation S16)}$$

where $\frac{p_{R_x}(t+dt)}{p_c(t+dt)}$ and $\frac{p_{R_x}(t)}{p_c(t)}$ represent *p(t+dt)* and *p(t)* respectively, in Equation S1. Thus, by dividing every *ex vivo* response curve by the corresponding vehicle control we are able to discard *ex vivo* spontaneous cell death and quantify direct drug-induced cell death. The parameters can then be estimated using MATLAB's *lsqcurvefit*, which minimizes the sum of squares of the residual (difference between normalized *ex vivo* data and the model estimate) at every data point. The *ex vivo* data consists of percent live cells normalized by control at 0 hours, drug concentration, and exposure time. Our objective is to estimate the set of parameters that best fit this data using the least squares method. Further, we used Akaike Information Criterion[8] (AIC)

$$AIC = 2k + n \ln\left( SSR / n \right), \quad \text{(Equation S17)}$$

where SSR is the sum of squares of residual, n is the number of data points used for estimation, and k is the total number of parameters used to describe the model. The model with the smallest AIC is considered to be the best model.

**Supplemental Figures and Tables:**

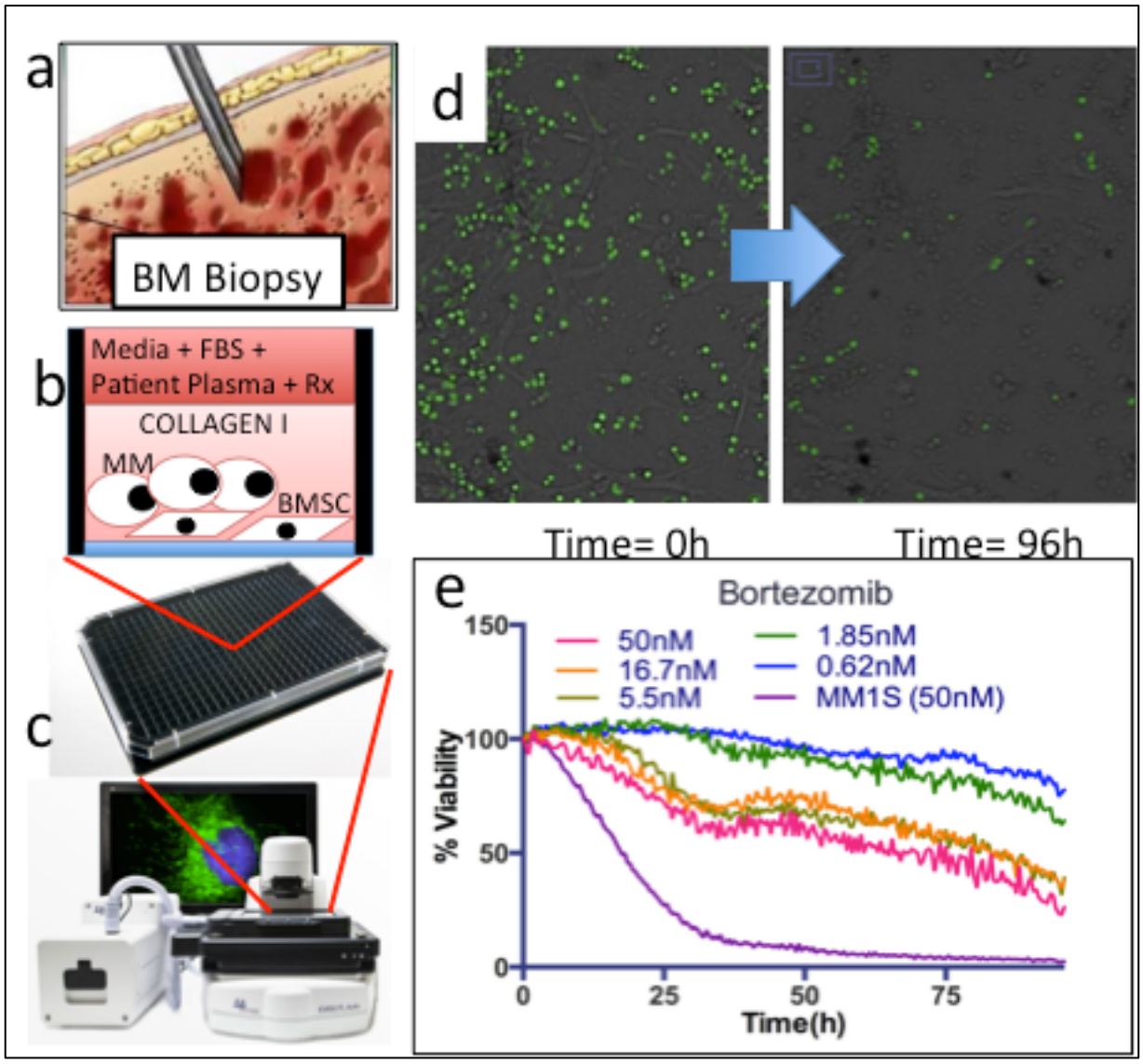


**Supplemental Figure 1. Overall workflow of ex vivo chemosensitivity assay.** During a standard-of-care bone marrow biopsy myeloma cells are separated from non-cancer by CD138-positive magnetic bead sorting. (a) Cancer cells are re-suspended in collagen-I in conjunction with stroma (adherent non-cancer cells obtained from bone marrow biopsies, CD138-). (b) The cell-matrix mix is seeded in a multi-well plate and left to polymerize overnight. Wells are organized so that 31 drugs can be tested at 5 different concentrations with 2 replicates. (c) By imaging at regular intervals each well in bright field, and using a digital image analysis algorithm, we non-destructively detect live and dead cells (d). (e) Digital image analysis algorithm quantifies longitudinal changes in number of live MM cells in each well and generates dose-response curves for each of the five concentrations plus the positive control (cell line MM1.S under highest concentration only).

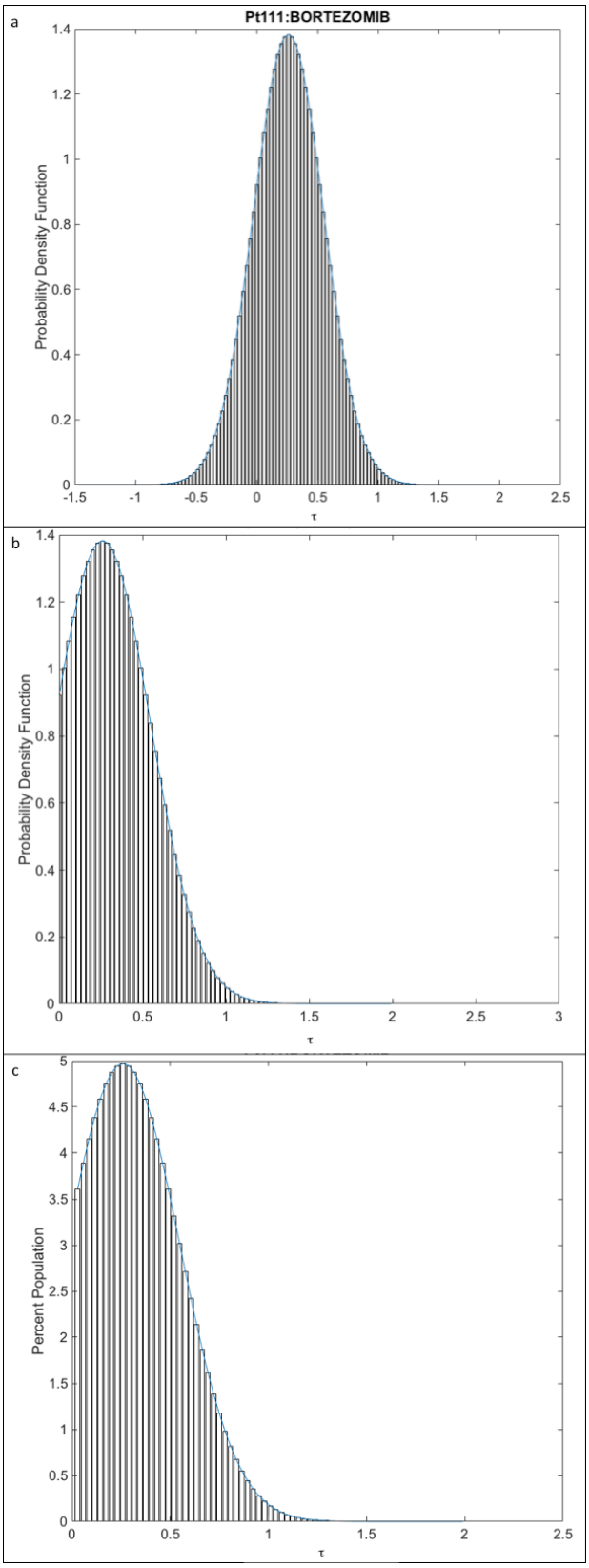


**Supplemental Figure 2. Computational implementation of tumor sensitivity as a probability distribution.** In the example above, patient Pt111's bortezomib sensitivity was best represented as a single mode normal distribution with regards to the threshold variable t. The distribution was approximated to a histogram spanning 12 standard deviations, with 10 bins per standard deviation (**a**). Since t is a positive value, the distribution is truncated to remove negative values for t (**b**). To ensure that the sum of all bins amounts to 100%, we multiply each bin by the sum of all bin values and multiply by 100% (**c**).

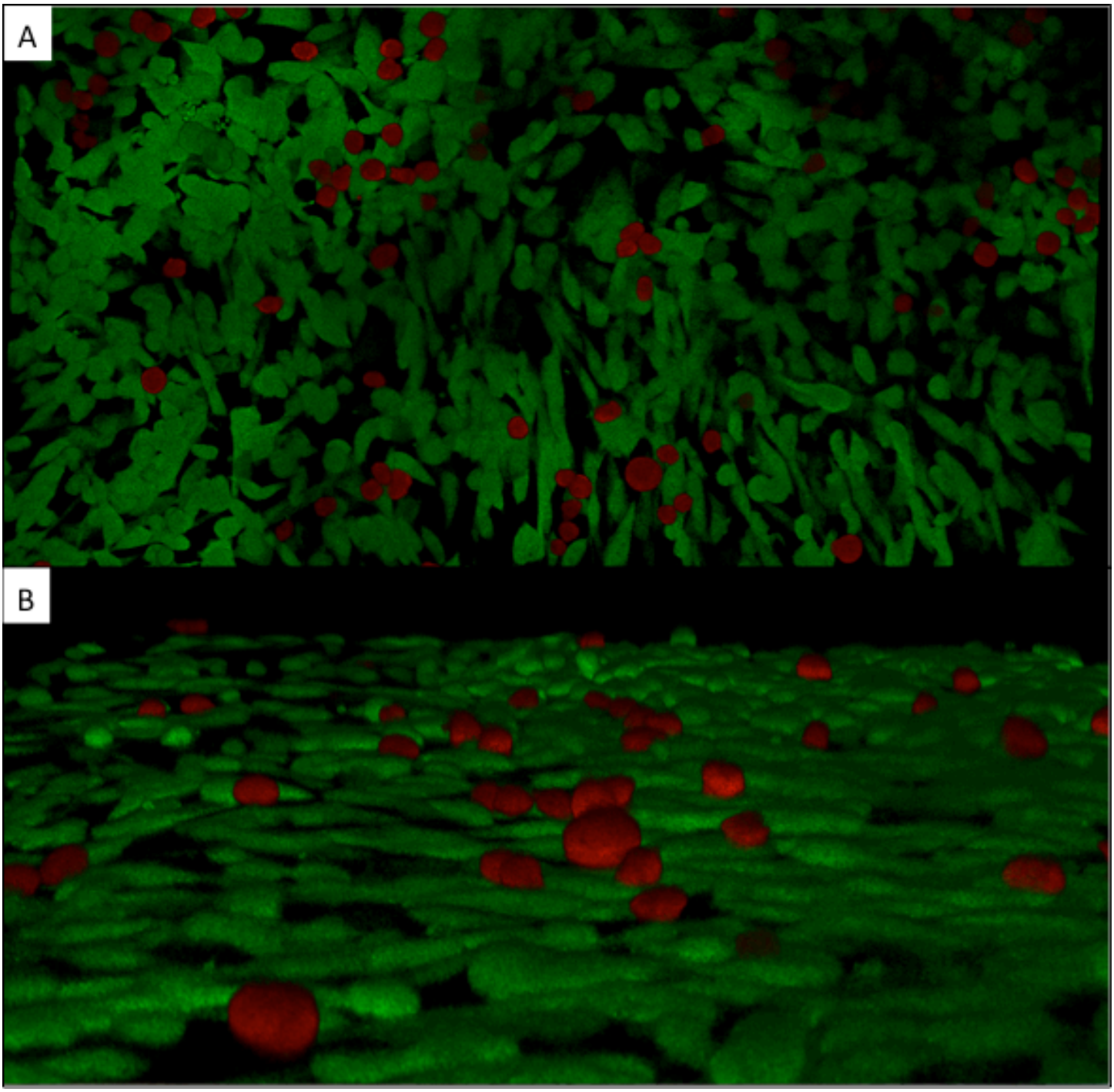


**Supplemental Figure 3. Spatial co-localization of MM and stroma.** Confocal microscopy of co-culture of stably transfected human myeloma cell line 8226/dsRed2 and human stromal cell line HS-5/GFP confirm that MM cells maintain a round shape while stroma stretches and adheres to bottom of well (A) while both populations maintain close contact and adhesion (B).

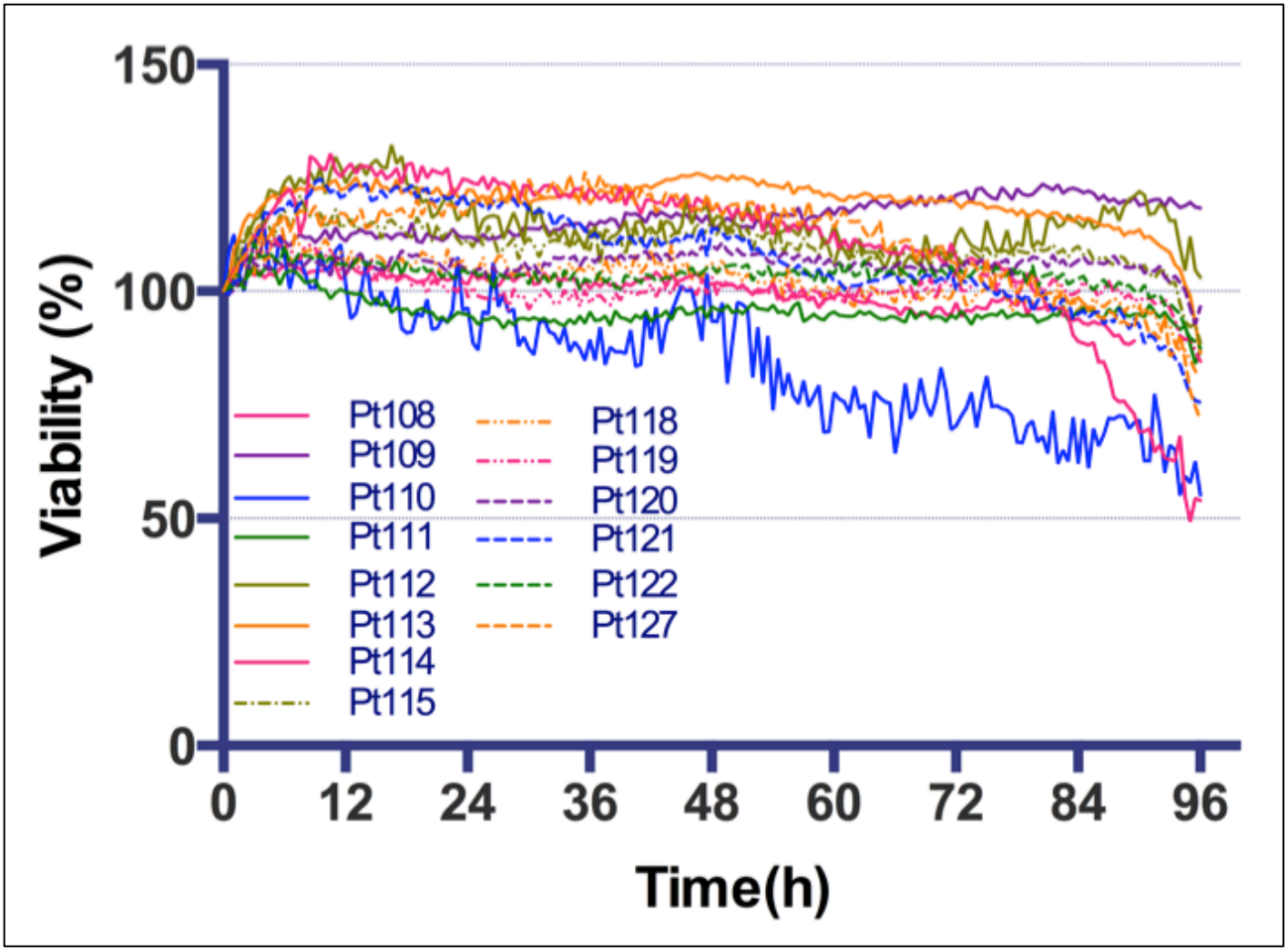


**Supplemental Figure 4. Example of assessment of spontaneous cell death in 14 primary MM samples across 96h in EMMA's ex vivo assay.** Please note the border effect artifact that suggests increase in viability in the beginning of the experiment, and decrease at the end. This border effect is removed when the curves from each experimental condition is divided by the corresponding controls. In the examples above, only the samples from patients Pt108 and Pt110 had a significant rate of spontaneous cell death, while the remaining patients had less than 25% loss of viability under control conditions.

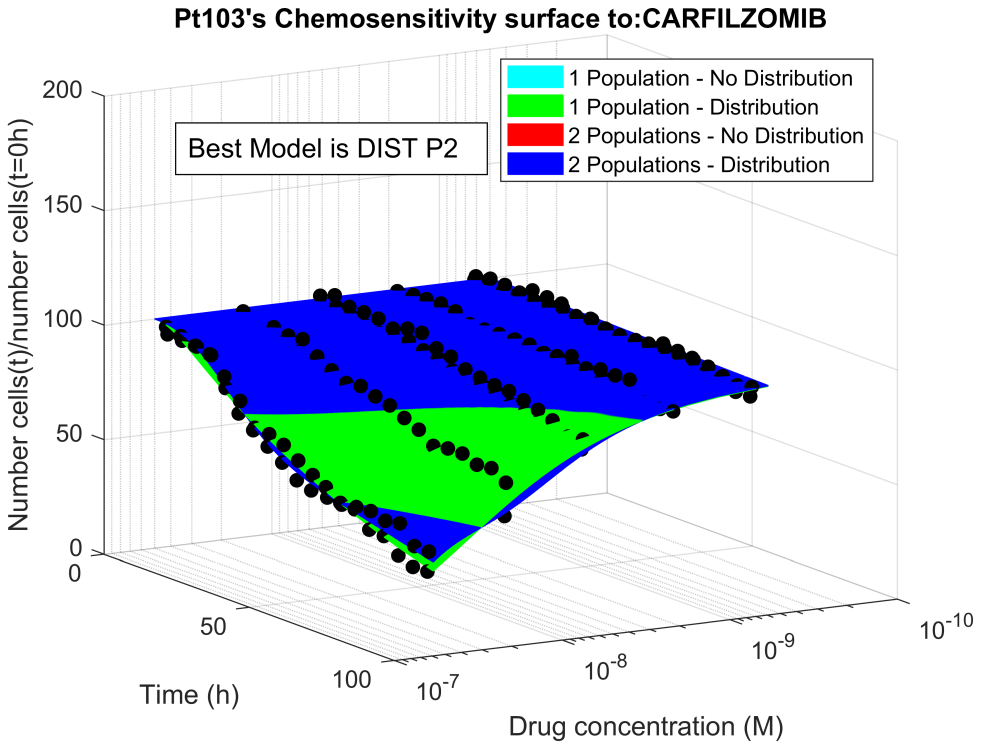


**Supplemental Figure 5. Ex vivo chemosensitivity curve of patient Pt103 to carfilzomib.**

| Parameter | Obtained from | Used in | Value |
|---|---|---|---|
| $LI$ | Previous relapse or 1% if naïve | Eq. (S3) | 1.44% |
| $a_1, \mu_1$ | Ex vivo assay | Eq. (S10) | 8.0139e-3 |
| $a_2, \delta_1$ | Ex vivo assay | Eq. (S9) | 7.3421e-4 |
| $a_3, \kappa$ | Ex vivo assay | Eq. (S4) | 0.012432 |
| $a_4, h$ | Ex vivo assay | Eq. (S4) | 0.4669 |
| $a_5, \sigma_1$ | Ex vivo assay | Eq. (S10) | 4.007e-3 |
| $a_6, p_1$ | Ex vivo assay | Eq. (S14) | 47.098% |
| $a_7, \mu_2$ | Ex vivo assay | Eq. (S10) | 0.024996 |
| $a_8, \sigma_2$ | Ex vivo assay | Eq. (S10) | 6.3511e-3 |
| $a_9, \delta_2$ | Ex vivo assay | Eq. (S9) | 5.4014e-4 |

**Supplemental Table 1. Model parameters for patient Pt103's primary MM cells tested ex vivo with carfilzomib.**

**Supplemental Figure 6. Correlation between predicted trajectories and actual clinical response of 52 MM patients up to 90 days post biopsy.**
Please see document with 52 pages, one for each patient.

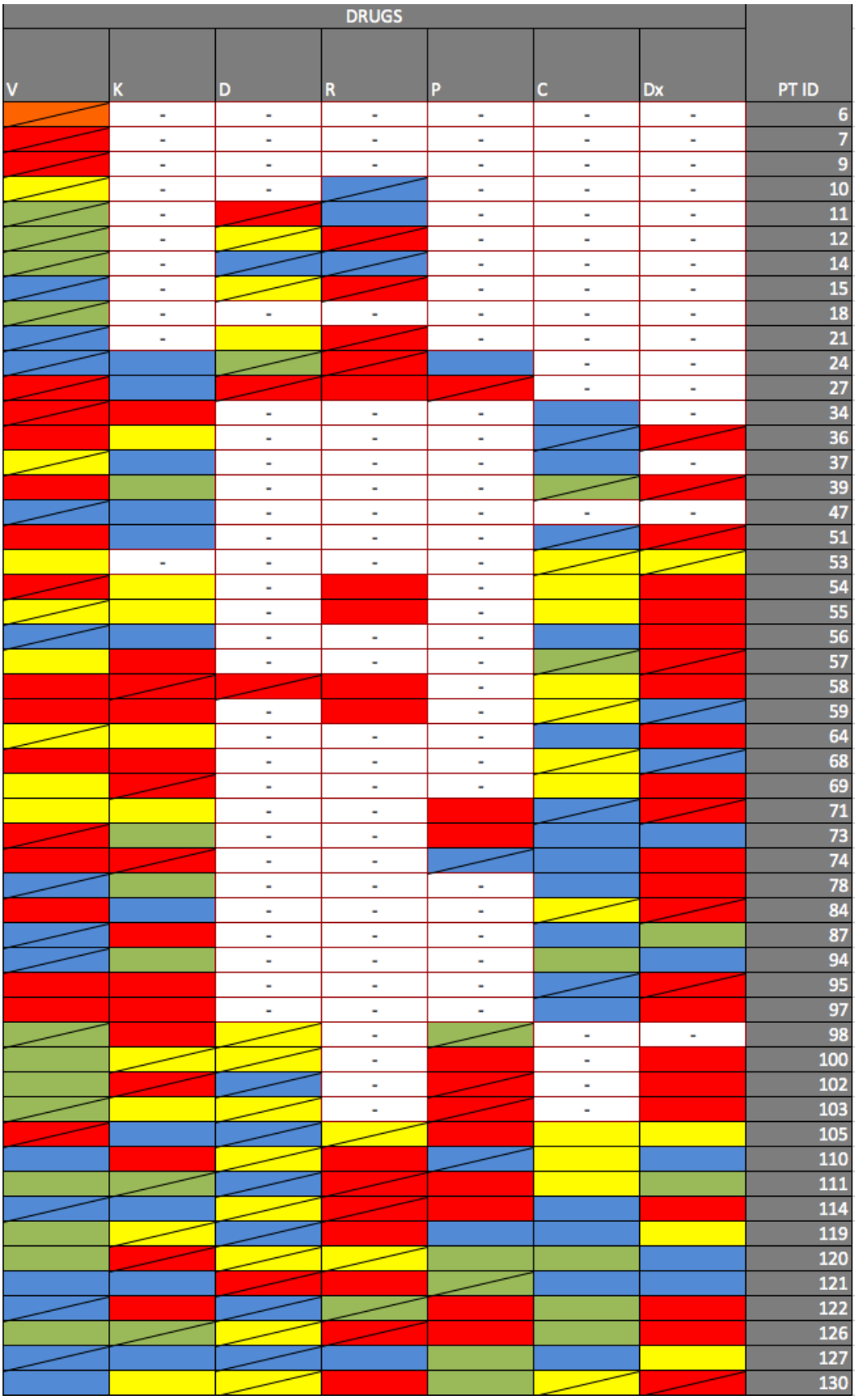


**Supplemental Table 2. Choice of best therapeutic option based on EMMA.** The above table groups the clinical predictions of the 52 MM patients in this study for 7 individual drugs: bortezomib (V), carfilzomib (K), dexamethasone (D), lenalidomide (R), pomalidomide (P), CRM1i (C) and doxorubicin (Dx). Each prediction is color coded as follows: green for VGPR/CR, orange for MR/PR, yellow for SD, and red for PD. Drugs that were not tested *ex vivo* for a patient sample appear as white. Diagonal lines mark the drugs that were actually administered to the patients. This dataset suggests that approximately 40% of the agents administered to these patients had no clinical efficacy (diagonal marked red cells). In addition, the model predictions suggested a different therapeutic choice, with deeper response, for 16 patients (27, 34, 37, 64, 69, 73, 78, 84, 87, 94, 100, 102, 119, 120, 127 and 130).

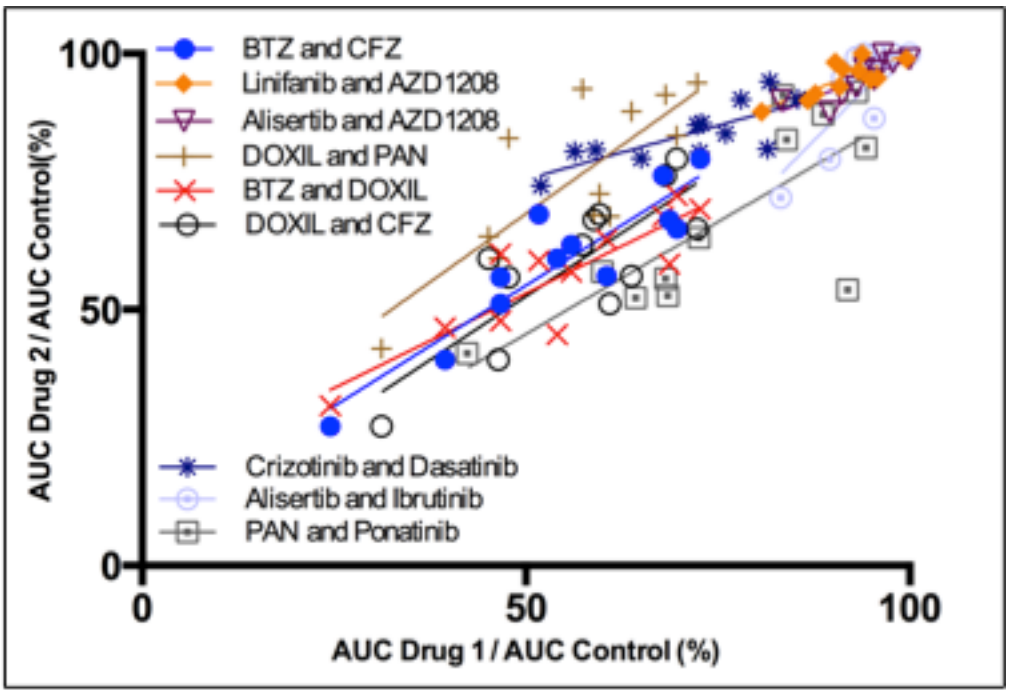


**Supplemental Figure 7. Correlation between *ex vivo* drug efficacy in 12 MM patients tested with six chemotherapeutic agents and 25 PKIs.** We have paired the 31 agents and calculated the linear regression of area under the curve (AUC) across 12 MM patients in order to determine correlation of drug sensitivity. The top correlations are depicted in the figure: bortezomib and carfilzomib (Pearson r=0.9141), bortezomib and doxorubicin (r=0.8762), linifanib and azd1208 (r=0.8322), doxorubicin and carfilzomib (r=0.8136), doxorubicin and panobinostat (r=0.8046), crizotinib and dasatinib (r=0.7764), alisertib and azd1208 (r=0.7752), alisertib and Ibrutinib (r=0.7749) and panobinostat and ponatinib (r=0.7694).

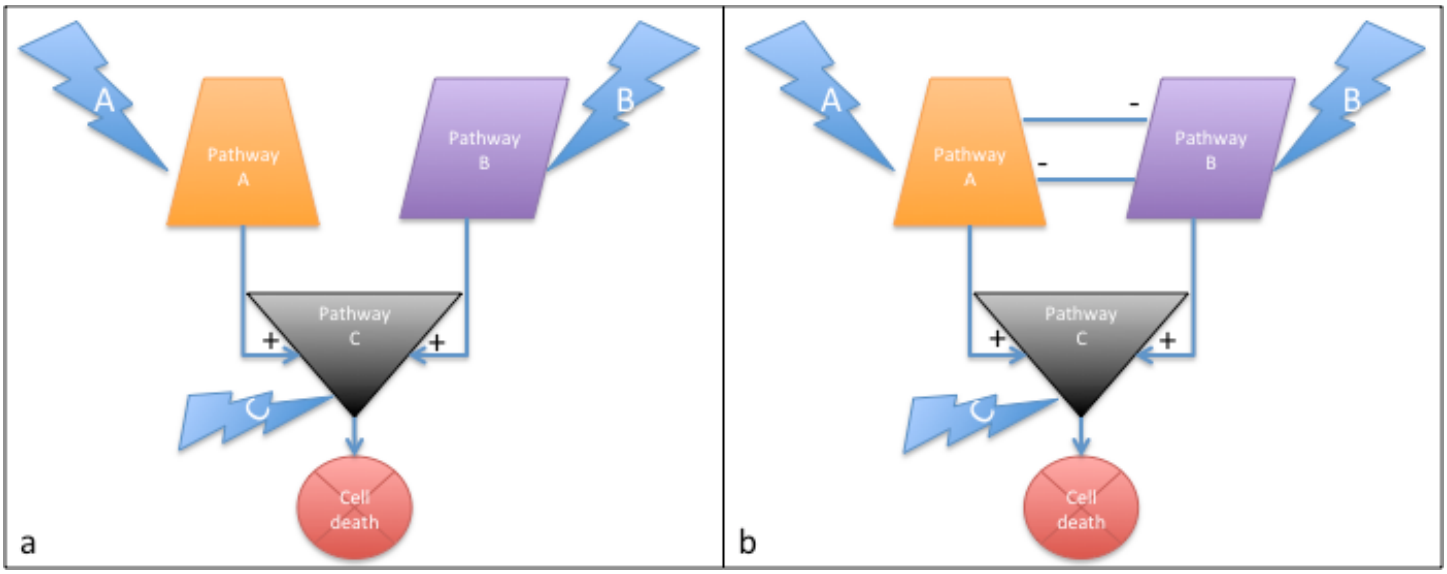


**Supplemental Figure 8. Hypothetical models for inter-patient correlation of drug sensitivity.** (**a**) Consider two independent pathways, A and B, converging downstream into pathway C. Drugs that target any of these pathways can cause cell death. Cellular adaptations that downregulate pathway C will make the cell resistant to drugs that target this pathway and also cross-resistant to those upstream (A and B). In other words, resistance to drugs that target pathway C will correlate with resistance to drugs that target either A or B, and vice versa. While (**a**) is a common motif in intracellular cell signaling, and explains the commonly observed development of cross-resistance observed in patients in the clinic, the explanation of cross-sensitivity, or increase in sensitivity to one drug as a consequence of increase in resistance to another, requires a more complex motif (**b**). In this network, once again pathway C is downstream from A and B, but now pathways A and B suppress each other. Thus, mutations that downregulate the effect of pathway A will cause upregulation of pathway B and thus increase in sensitivity to drugs targeting pathway B. This is a less common motif and possibly explains the lack of drugs with negative correlation of sensitivity in the panel of 25 PKIs studied in this work.

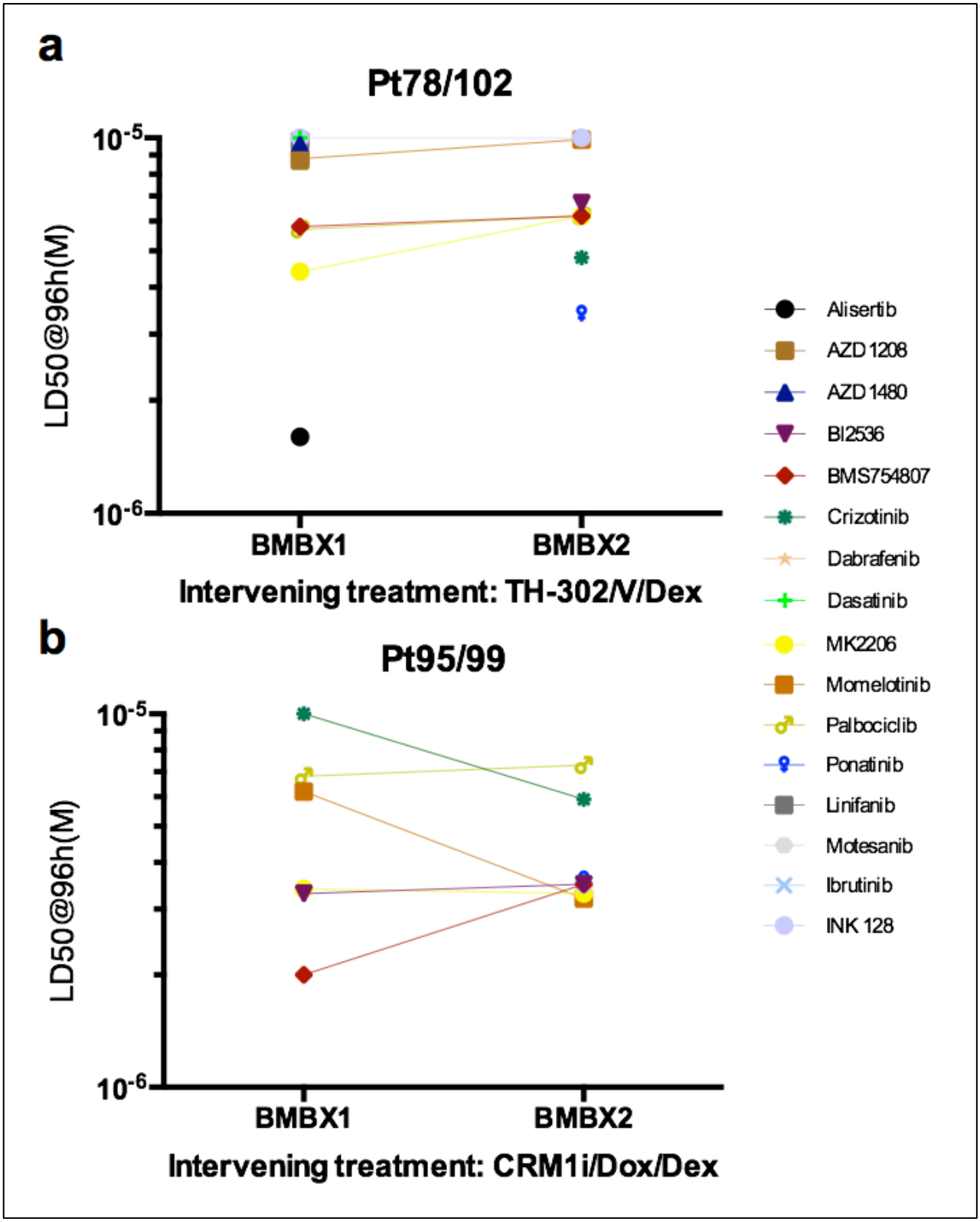


**Supplemental Figure 9. Changes in chemosensitivity of tumor cells from two MM patients to 20 PKIs between two sequential biopsies.** Each marker represents the LD50 at 96h for a particular combination of patients/biopsy. When LD50 is not reached, the marker is absent. For 4 PKIs (Ruxolitinib, Selumetinib, Tozasertib and Trametinib), the LD50 at 96h was higher than me maximum concentration tested (10µM) and thus could not be determined. (a) This patient provided two biopsies separated by an interval of 4 months, during which the patient was treated with a combination of the hypoxic pro-drug TH-302, bortezomib and dexamethasone. Some PKIs were more effective in the first biopsy than in the second (e.g. Alisertib and Dasatinib) while others only more efective in the second biopsy (e.g. Ponatinib, Crizotinib and BI2536). (b) This patient provided two biopsies separated by three weeks, during which the patient was treated with the nuclear export inhibitor selinexor, liposomal doxorubicin and dexamethasone. The most noticeable increases of sensitivity were Crizotinib and Momelotinib, and the most noticeable increase in resistance was BMS754807.

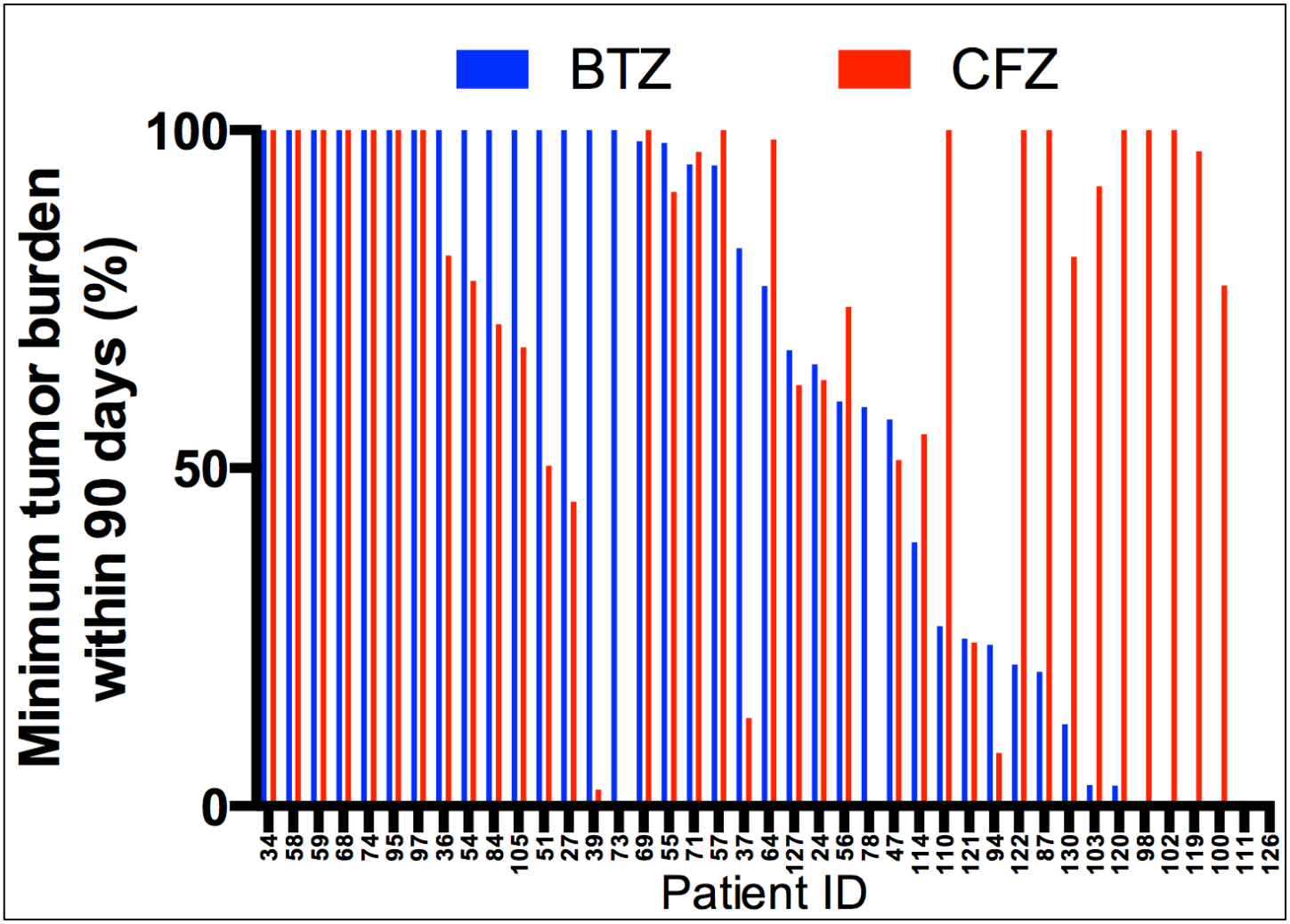


**Supplemental Figure 10. Model predictions of 41 MM patients indicate no correlation between bortezomib and carfilzomib 90-day depth of response.** For each patient, the blue and red lines represent the minimum tumor burden expected in a 90-day treatment with single agent bortezomib and carfilzomib, respectively. Patients have been sorted from left to right in descending order of clinical resistance to bortezomib.

| Patient ID | Status at biopsy | Age | Sex | Race | t(11:14) |
|---|---|---|---|---|---|
| 127 | NDMM | 58 | Female | Black or African American | NO |
| 129 | Triple | 60 | Male | Black or African American | NO |
| 130 | Quad | 76 | Male | White | NO |
| 135 | Naïve | 70 | Female | White | NO |
| 138 | Naïve | 60 | Male | White | NO |
| 140 | NDMM | 68 | Male | White | YES |
| 141 | PI-R | 62 | Male | White | NO |
| 142 | NDMM | 75 | Male | White | YES |
| 143 | PI-R | 66 | Female | White | NO |
| 144 | Naïve | 69 | Female | White | NO |
| 145 | Double | 55 | Female | White | NO |
| 148 | Triple | 54 | Female | White | YES |
| 152 | NDMM | 69 | Male | White | NO |
| 160 | NDMM | 45 | Male | White | NO |
| 161 | Naïve | 60 | Male | White | YES |
| 163 | Double | 73 | Female | White | NO |
| 164 | Triple | 52 | Male | Other | NO |
| 165 | Naïve | 68 | Male | White | NO |
| 166 | Penta | 69 | Female | White | YES |

**Supplemental Table 3. Demographics of patients whose bone marrow aspirates were used in virtual clinical trials of ricolinostat and venetoclax.** Status at bone marrow biopsy were: newly diagnosed (NDMM), proteasome inhibitor resistant (PI-R), double-refractory, triple-refractory, quad-refractory, penta-refractory, and naïve (relapse in absence of therapy). Patients were also classified according to presence of translocation 11,14 in standard of care MM FISH.

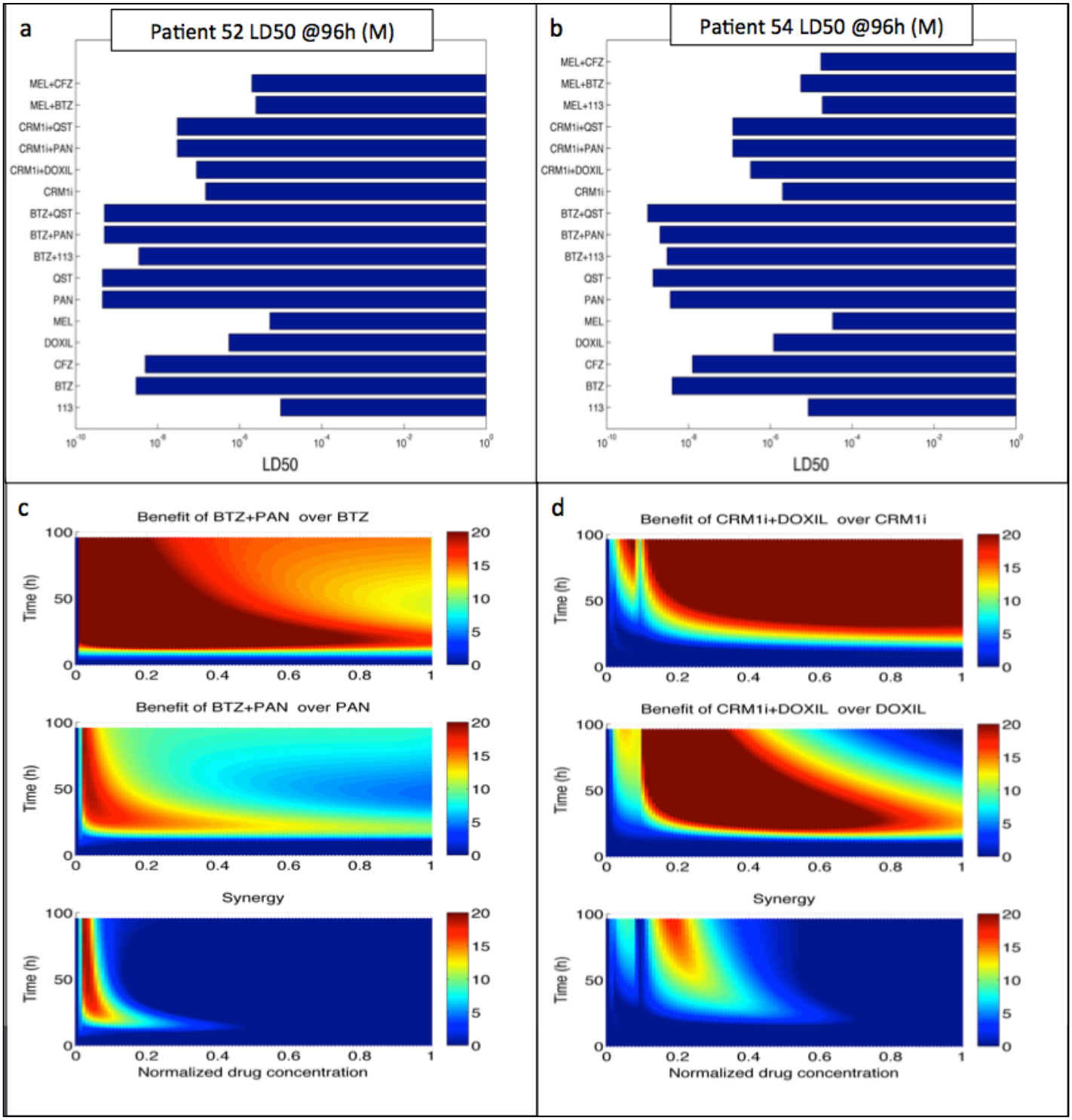


**Supplemental Figure 11. Quantification of drug sensitivity and time-dependent synergy in primary MM cells.** (**a**) and (**b**) represent the LD50 (concentration for 50% reduction in viability as compared to the beginning of experiment, normalized by control) of primary MM cells from two patients. Please note that for drug combinations, only the LD50 of the first drug is shown. (**c**) and (**d**) show a more detailed representation of drug efficacy across concentration and exposure time, revealing the concentrations where drug combinations increase cell kill, and identifying possible synergy "islands", where effect of the drug combination is higher than the product of their individual efficacies. List of drugs tested ex vivo: MEL (melphalan), CFZ (carfilzomib), BTZ (bortezomib), CRM1i (selinexor), QST (quisinostat), PAN (panobinostat), DOXIL (liposomal doxorubicin) and 113 (defactinib).

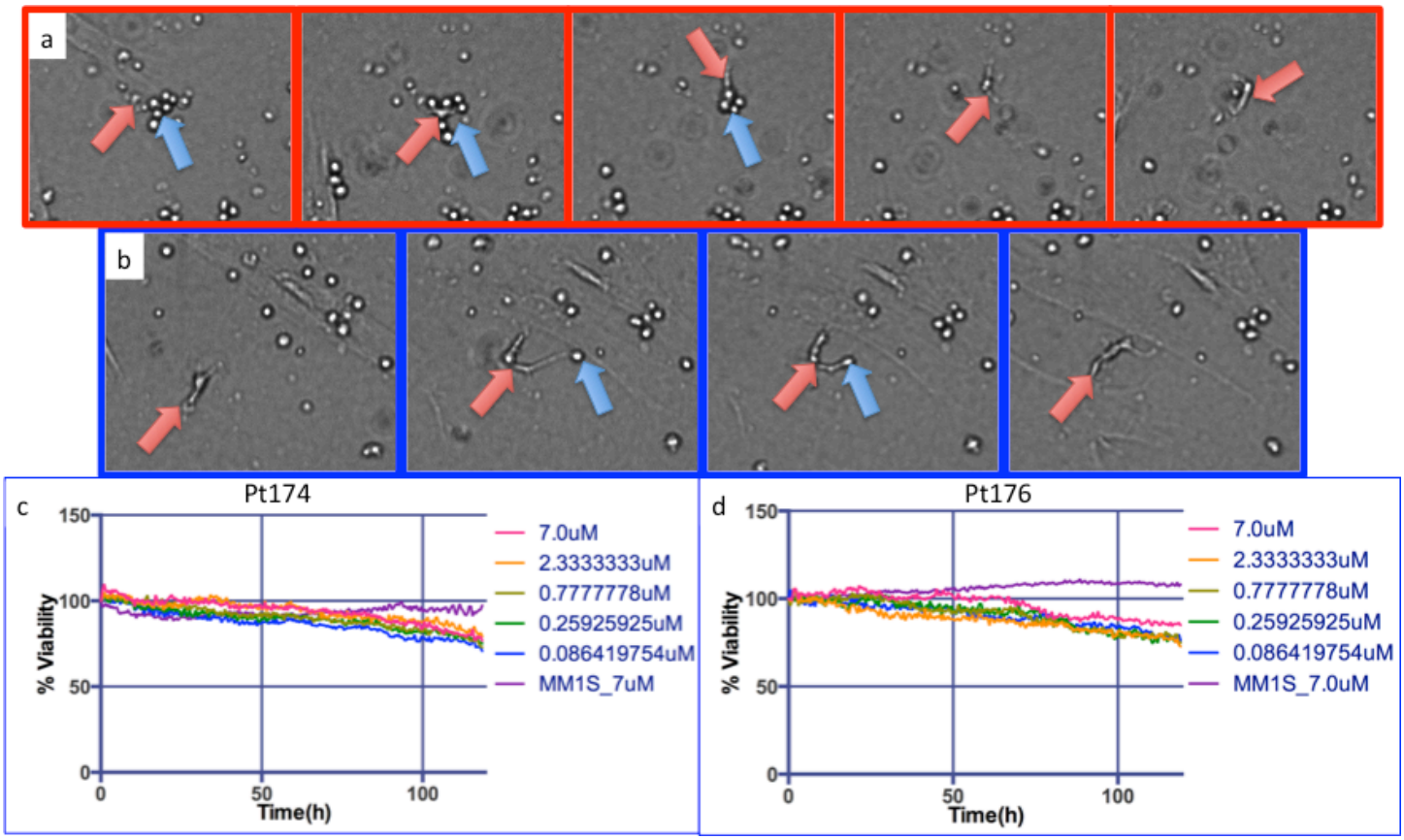


**Supplemental Figure 12. Daratumumab-mediated MM cell death.** Unlike drugs with direct cytotoxic activity studied in this manuscript, daratumumab, a CD38 monoclonal antibody[9,10], mediates immune response to MM cells. The first and second panels (**a** and **b**) depict two separate groups of MM cells from patient Pt174 (blue arrow) during an EMMA assay, exposed to 7μM of daratumumab for 120h. After approximately four days of exposure, a yet-to-be-determined adherent cell (red arrow), originated from either the patient aspirate or stroma, begins to engulf the MM cells in its vicinity, and proceeds to other regions of the well. This process is observed in all wells with daratumumab, from concentrations 7μM to 86nM; it does not occur in controls, and was observed in two separate patients (**c**).

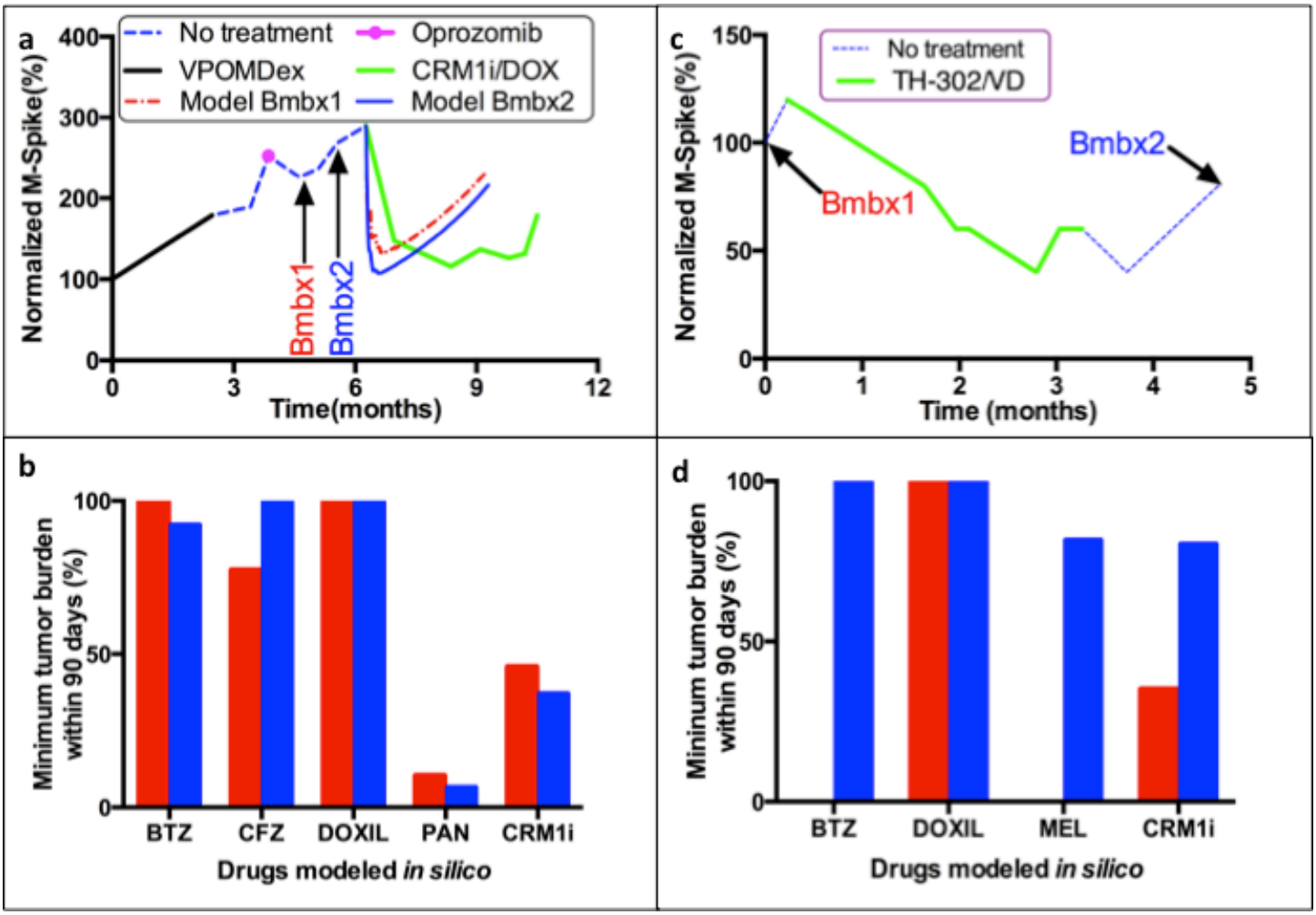


**Supplemental Figure 13.** ***Ex vivo*** **chemosensitivity in sequential biopsies in absence and during treatment.** (**a**) To assess the inter-day reproducibility of the *ex vivo* assay (test-retest) we have quantified the chemosensitivity of one patient (**Pt52**) with two biopsies separated by one month without treatment and used this information to build mathematical models of predicted clinical response to therapy (CRM1i) using the *ex vivo* data from both biopsies (red dashed line for biopsy 1, blue solid line for biopsy 2), indicating high correlation between both modeled curves (Pearson r=0.9707) and thus reproducibility of assay. (**b**) Variation of mathematical model clinical predictions of best response built with *ex vivo* data from two sequential biopsies (**Pt52**). (**c**) Two biopsies of patient **Pt32**, separated by treatment with Th-302, bortezomib and dexamethasone, were tested for *ex vivo* chemosensitivity (this patient had the dose of bortezomib reduced from 1.3mg/m$^2$ to 1mg/m$^2$ due to thrombocytopenia). (**d**) Model predictions indicate that the patient, who was initially sensitive to proteasome inhibitors and alkylating agents, has become refractory to both.

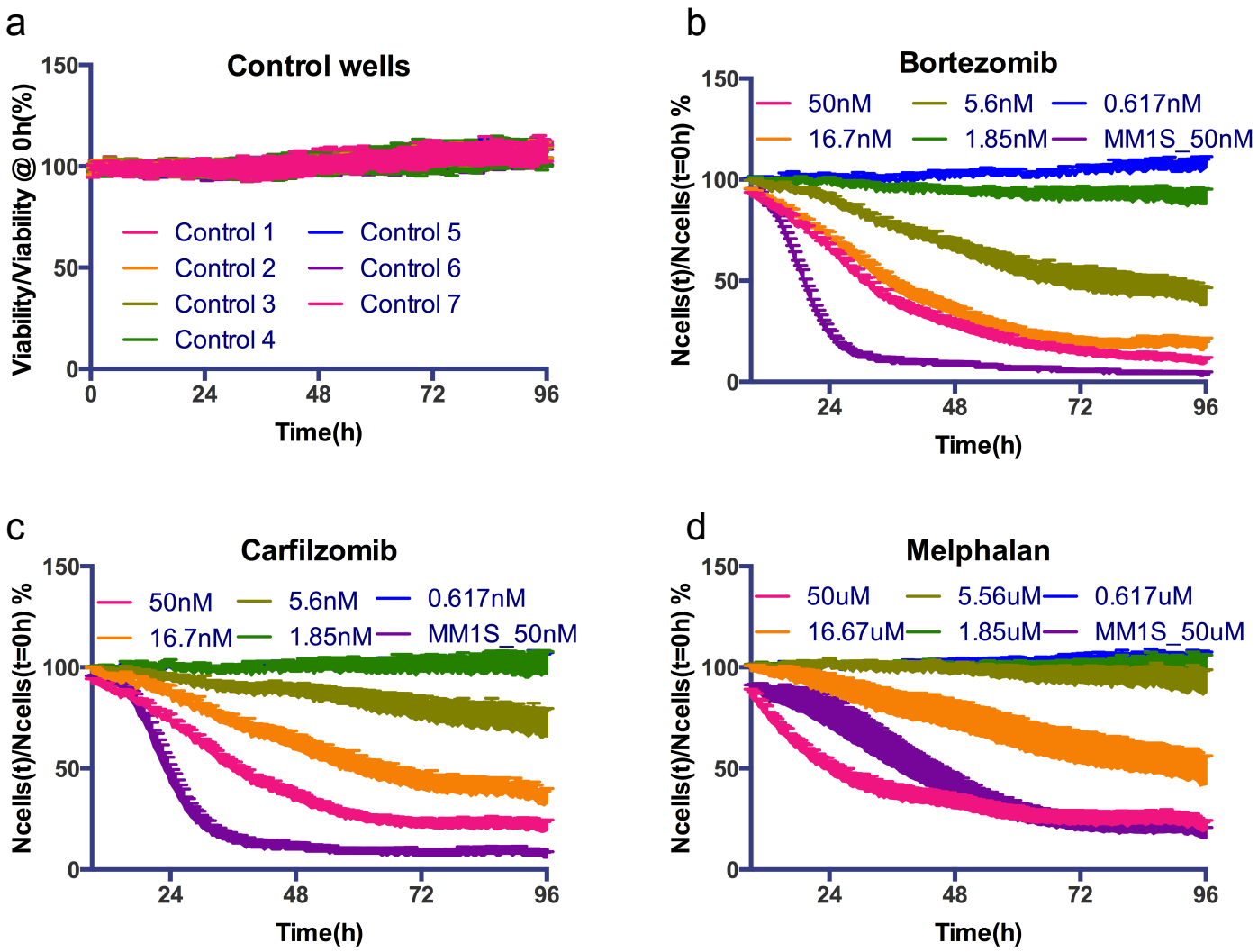


**Supplemental Figure 14. Intra-plate variation of *ex vivo* assay.** Primary cells from a patient (Pt48) were seeded as usual in a 384-well plate and tested in a pattern of three different drugs (bortezomib, melphalan and carfilzomib), at five concentrations and two replicates, and a negative control (no drugs added). This pattern was repeated 8 times across the plate and standard deviation (S.D.) of dose response curves for each drug and concentration were determined. Maximum S.D. values were 3.4% for melphalan, 6.3% for bortezomib, 8.9% for carfilzomib, and 6.7% for controls.

## 1 Population – No Distribution

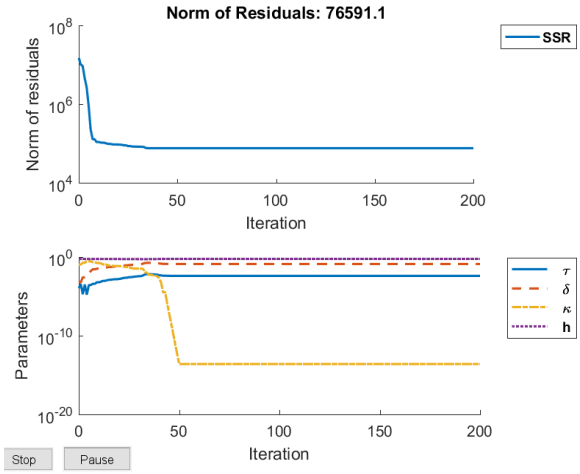


## 2 Populations – No Distribution

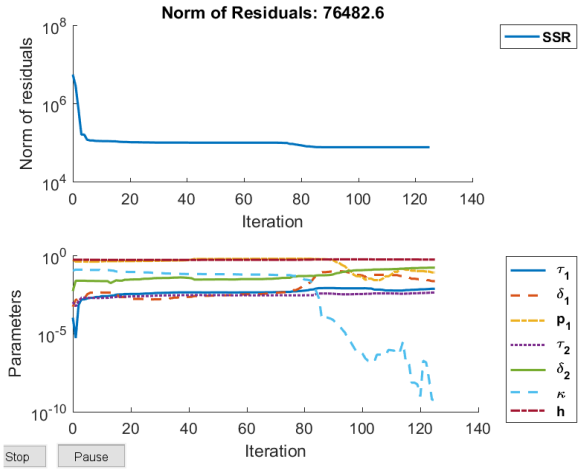


## 1 Population – Distribution

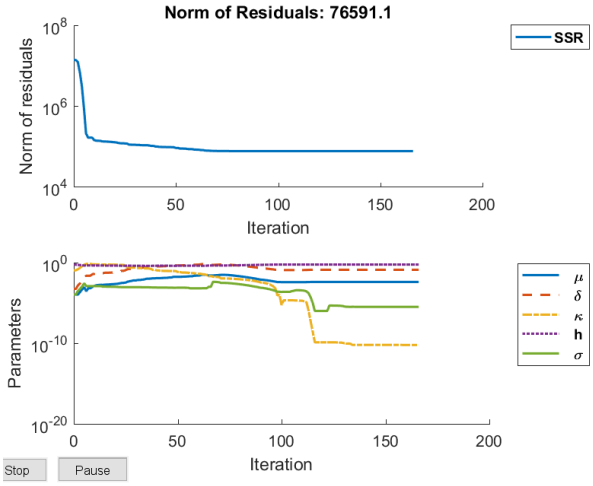


## 2 Populations – Distribution

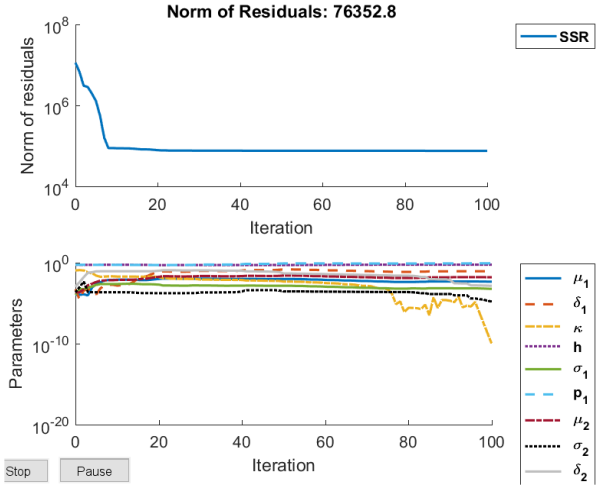


**Supplemental Figure 15. Convergence study comparing the four population models for panobinostat.**

| | 1 Pop – No Dist. | 2 Pops – No Dist. | 1 Pop – Dist. | 2 Pops – Dist. |
|---|---|---|---|---|
| Sum of Squares of Residuals (SSR) | 76,591.1 | 76,482.6 | 76,591.1 | 76,352.8 |
| Number of parameters (k) | 4 | 7 | 5 | 9 |
| Akaike Information Criterion (AIC) | 76.2234 | 76.2533 | 76.2434 | 76.2572 |

**Supplemental Table 4. SSR, number of parameters, and AIC values for the four models for patient Pt103's *ex vivo* sensitivity to panobinostat.**

## 1 Population - No Distribution

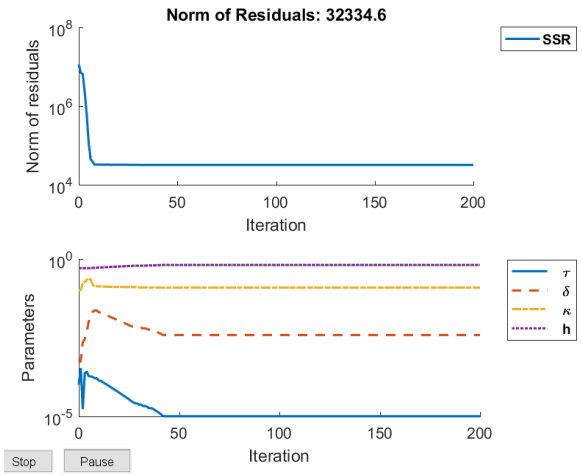


## 2 Populations - No Distribution

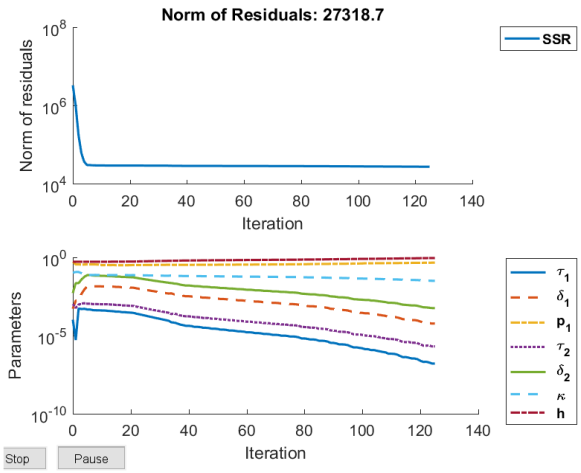


## 1 Population - Distribution

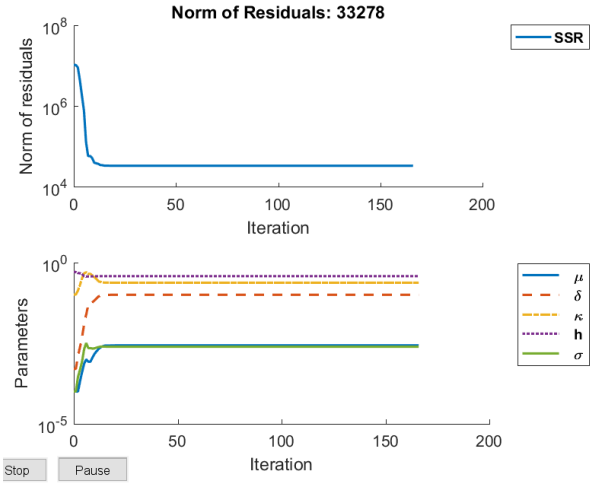


## 2 Populations – Distribution

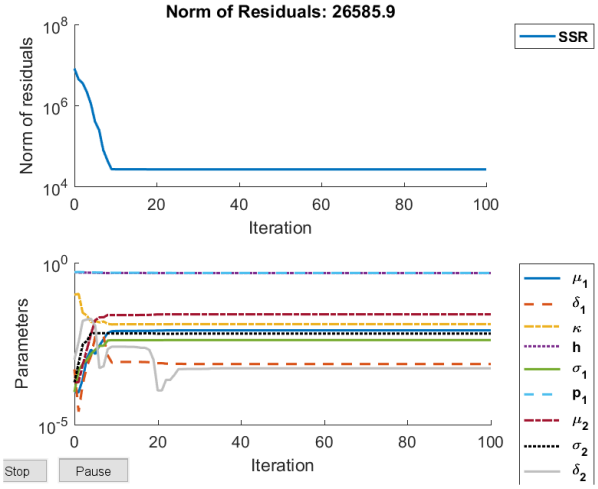


**Supplemental Figure 16. Convergence study comparing the four population models for carfilzomib.**

| | 1 Pop – No Dist. | 2 Pops – No Dist. | 1 Pop – Dist. | 2 Pops – Dist. |
|---|---|---|---|---|
| Sum of Squares of Residuals (SSR) | 32,334.6 | 27,318.7 | 33,278.0 | 26,585.9 |
| Number of parameters (k) | 4 | 7 | 5 | 9 |
| Akaike Information Criterion (AIC) | 57.9158 | 54.3972 | 58.5464 | 53.8599 |

**Supplemental Table 5. SSR, number of parameters, and AIC values for the four models for carfilzomib.**

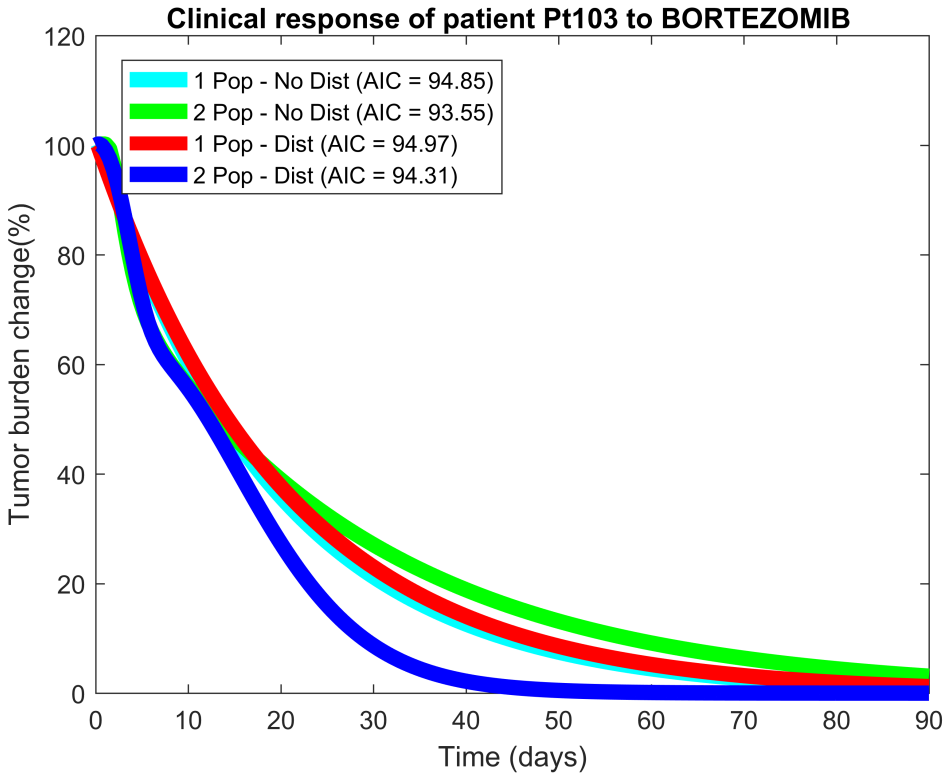


**Supplemental Figure 17. Comparison between clinical predictions for bortezomib using the four models.**

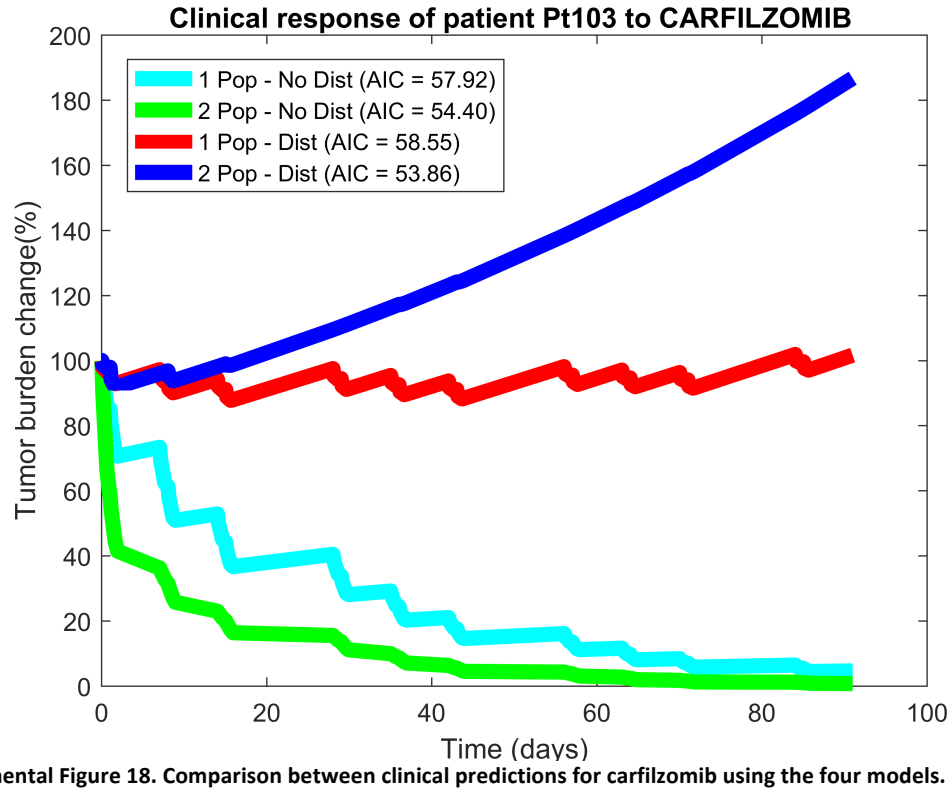


**Supplemental Figure 18. Comparison between clinical predictions for carfilzomib using the four models.**

**Data Processing Guide:**

The flow of data analysis consists in multiple steps: (a) running the digital image analysis algorithm in imageJ; (b) creation of a description file assigning each well in the plate to a particular drug and concentration; (c) grouping the results from image analysis of wells according to drugs and concentrations, normalizing results by control and time 0h; (d) creation of charts in Prism Graphpad format; and (e) generation of Matlab code for analysis of chemosensitivity as well as estimates of clinical response. These steps are automated by different pieces of software developed in Javascript (for ImageJ), Java and Matlab, and are provided below.

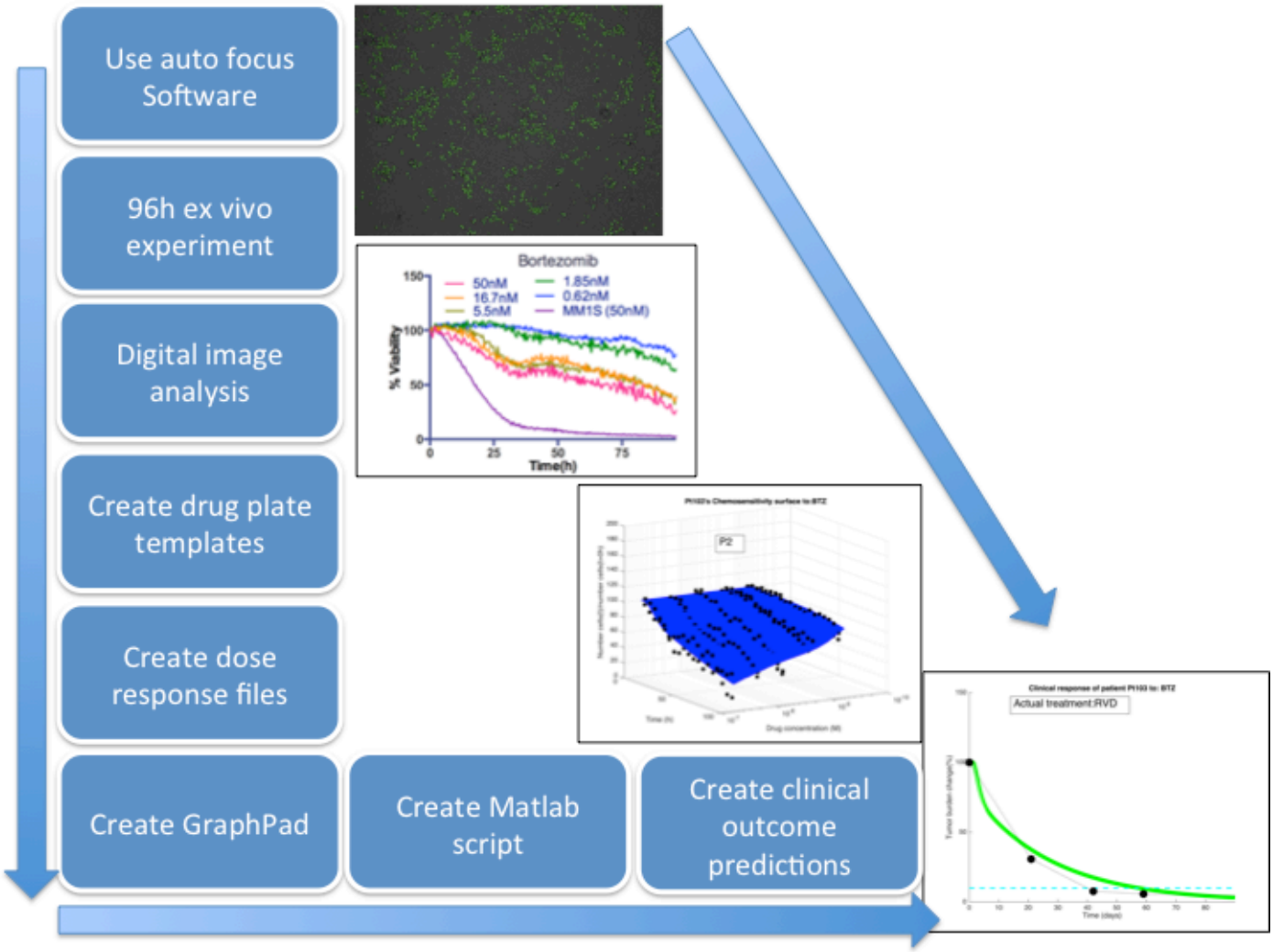

# Use auto focus software

- Open template file with pre-defined beacons;
- Set beacons 1, 24, 180, 181, 361 and 384;
- Run time lapse and stop after at least one beacon was imaged;
- Save results;
- Open template file using software CalibrateFocus.jar (below, arrow 1)

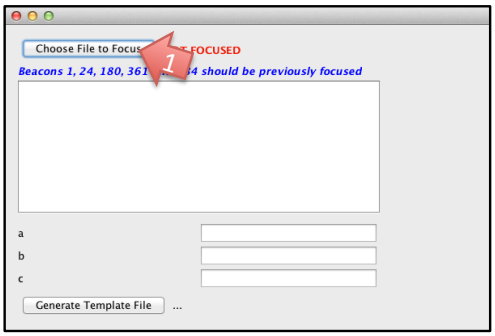


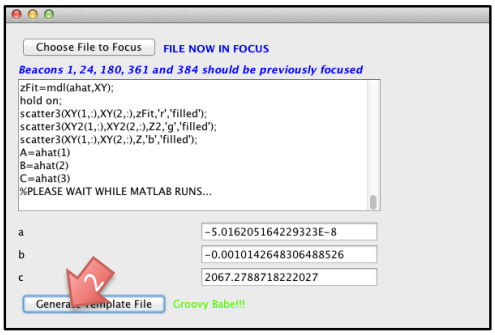


- One the file is read, the software will calculate the correct focal “plane”;
- Press the “Generate template file” and close the software;
- Re-open the now focused template file in and run the time lapse;

# Digital image analysis

- Copy the folder containing all beacons into cluster's "parent folder";
- Open the file BatchGenerator.sh and change the value of the property "folder" to the name of the folder containing all the beacons;
- Open the file BatchStart.txt and edit the path imageJ, imageJ script and "parent folder" where the folder with beacons are stored:
  - Default imageJ path: /home/silvaa/fiji
  - Default imageJ macro path: /home/silvaa/fiji/macros/MacroAnalysis384_14Cluster.ijm
  - Default "parent folder" containing all beacons: /share/data/evos_silva**/$folder/Beacon-$beacon**
- **Do not replace the text in red.**
- Run the analysis with the command line: bash ./BatchGenerator.sh
- Once the jobs are completed, a folder named "tiffs" will be created inside the "folder" directory. Inside "tiffs" there will be a video for each beacon as well as a results.csv file with the time lapse analysis of all beacons;

# Create drug plate templates

- Open the template file DrugList.csv;
- Edit the names of drugs in the file according to their spatial location in the drug plate used in the robotic plate handler;
- Modify the maximum concentration (final) for each drug. For instance, if the maximum concentration in the 384-well plate with cells is 10uM, then enter this value here;
- Run the software BuildExperimentalDesign.jar and pass as parameter the path to the folder containing the Druglist.csv file. For instance:
  - java -cp BuildExperimentalDesign.jar BuildExperimentalDesign "/Users/silvaa/Desktop/Pt in cluster/Pt101"
- The software creates two folders named "PtSample" and "MM1_S". The first contains the list of beacons and corresponding drug names and concentrations for the wells with primary cells, and the second for the cell line positive control. Each folder has a unique file name ExperimentalDesign.txt;

# Create dose response files

- Copy the file “results.csv” inside both “PtSample” and “MM1_S” folders;
- Run software Evos384.jar;

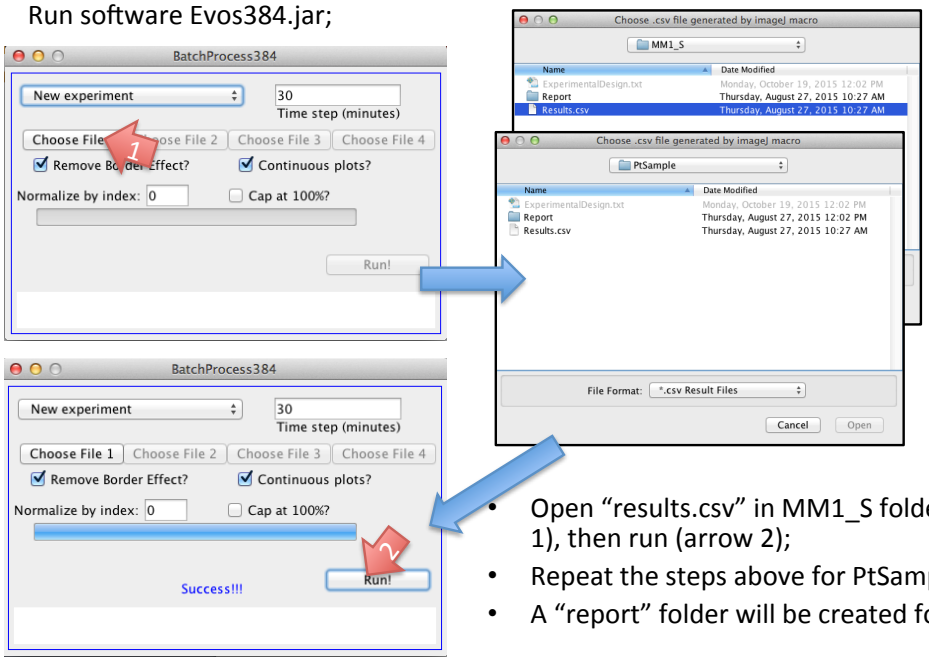


- Open “results.csv” in MM1_S folder (arrow 1), then run (arrow 2);
- Repeat the steps above for PtSample;
- A “report” folder will be created for each;

# Create GraphPad

- Run the software to build the GraphPad report and It will generate a file named Report.pzfx:
  - java -cp BuildGraphPadFile.jar BuildGraphPadFile "/Users/silvaa/Desktop/Pt in cluster/Pt101”
- Open the file using GraphPad and ignore the error message;
- Open the leaflet “info” and delete one of the two “Project info 1” items;
- Save the file with an alternative name, e.g. ReportPt101.pzfx;
- Re-open the file and there should be no error messages;
- Each of the 31 drugs and control should be depicted in a separate chart and numeric values in data tables;
- All values are normalized by negative controls and are 100% at timepoint 0h.

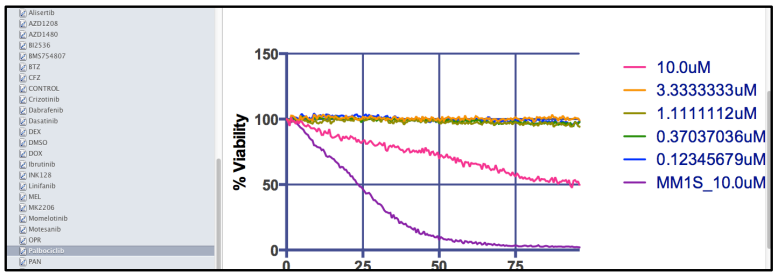

# Create Matlab script

- Run the software to build Matlab code for clinical predictions based on patient ex vivo results:
  - java -cp GenerateMatlabGraphFormat.jar GenerateMatlabGraphFormat "/Users/silvaa/Desktop/Pt in cluster/PtPathList.txt"
  - The file PtPathList.txt contains the folder where the Matlab script files will be stored (1) as well as the folders where each patient ex vivo results are stored (2). The syntax is: path to patient folder where ex vivo results are stored;-1;1;,;number of hours of experiment;patient identifier

```
/Users/silvaa/Desktop/Career/Manuscripts 2014/ModelingPredictionTherapyRes...e/Nature Medicine/Drug Synergy
/Users/silvaa/Desktop/Pt in cluster/Pt6/Report;-1;1;,;96;Pt6
/Users/silvaa/Desktop/Pt in cluster/Pt7/Report;-1;1;,;72;Pt7
/Users/silvaa/Desktop/Pt in cluster/Pt9/Report;-1;1;,;72;Pt9
/Users/silvaa/Desktop/Pt in cluster/Pt10+11/Pt10/Report;-1;1;,;90;Pt10
/Users/silvaa/Desktop/Pt in cluster/Pt10+11/Pt11/LenAsControl/Report;-1;1;,;90;Pt11
```

- The output will be the number of patients analyzed as well as any errors found:

```
Running.....Finished processing 57 patients.
```

- A file with each patient's ID will be created. To run the analysis, copy and paste code into Matlab

# Create clinical outcome predictions

- Run the software that creates a single Matlab script file for ex vivo, drug combination synergy and clinical outcome predictions for all patients:
  - java -cp DrugListSynergy.jar DrugListSynergy "/Users/silvaa/Desktop/Career/Manuscripts 2014/ModelingPredictionTherapyResponse/Nature Medicine/Drug Synergy"
  - Where the folder above contains the file DrugListSynergy.txt with the list of drugs and combinations to be modeled. Add new drugs to the bottom of the list.
  - A file named RunAllPatients.m will be generated. Copy this file to Matlab path and run the command RunAllPatients in Matlab's command line. Figures (.fig and .png) will be created in the folder */matlabFile*s:
    - Ptxx_DrugY_Clinical_Prediction: the treatmet simulation if there is an available PK model for the drug;
    - Ptxx_ClinicalRadar: bar plot with the minimum tumor, normalized by day 0, within an interval of 90 days, for the simulated drug as single agent;
    - Ptxx_ExVivo_DrugY: the ex vivo chemosensitivity dose response and fitting models;
    - Ptxx_ExVivoRadar: bar plot with AUC (area under curve) of dose response surfaces for the duration of the experiment;
    - Ptxx_LD50Radar: bar plot with LD50 concentrations (in molar) for the last time point of the experiment (default 96h);
    - Ptxx_Drug1+Drug2_Synergy: heatmaps comparing efficacy of drug combination versus either drug as single agent as well as conditions of synergy;

**Supplemental References:**


1. Winter, G.E.*, et al.* Systems-pharmacology dissection of a drug synergy in imatinib-resistant CML. *Nat Chem Biol* **8**, 905-912 (2012).
2. Hideshima, T., Richardson, P.G. & Anderson, K.C. Mechanism of action of proteasome inhibitors and deacetylase inhibitors and the biological basis of synergy in multiple myeloma. *Mol Cancer Ther* **10**, 2034-2042 (2011).
3. Turner, J.G.*, et al.* CRM1 Inhibition Sensitizes Drug Resistant Human Myeloma Cells to Topoisomerase II and Proteasome Inhibitors both In Vitro and Ex Vivo. *J Cancer* **4**, 614-625 (2013).
4. Chou, T.C. Drug combination studies and their synergy quantification using the Chou-Talalay method. *Cancer Res* **70**, 440-446 (2010).
5. Greco, W.R., Faessel, H. & Levasseur, L. The search for cytotoxic synergy between anticancer agents: a case of Dorothy and the ruby slippers? *J Natl Cancer Inst* **88**, 699-700 (1996).
6. Shargel, L., Wu-Pong, S. & Yu, A.B.C. *Applied biopharmaceutics & pharmacokinetics*, (Appleton & Lange Reviews/McGraw-Hill, Medical Pub. Division, New York, 2005).
7. Clark, A.J. The reaction between acetyl choline and muscle cells. Part II. *J Physiol-London* **64**, 123-143 (1927).
8. Akaike, H. New Look at Statistical-Model Identification. *Ieee T Automat Contr* **Ac19**, 716-723 (1974).
9. Jelinek, T. & Hajek, R. Monoclonal antibodies - A new era in the treatment of multiple myeloma. *Blood Rev* **30**, 101-110 (2016).
10. Lokhorst, H.M.*, et al.* Targeting CD38 with Daratumumab Monotherapy in Multiple Myeloma. *N Engl J Med* **373**, 1207-1219 (2015).